NORGES TEKNISK-NATURVITENSKAPELIGE
UNIVERSITET

A Globally Convergent Numerical Method for Some Coefficient Inverse Problems With Resulting Second Order Elliptic Equations

by

Larisa Beilina$^{\triangledown}$, Michael V. Klibanov*

PREPRINT
NUMERICS NO. 11/2007

NORWEGIAN UNIVERSITY OF
SCIENCE AND TECHNOLOGY
TRONDHEIM, NORWAY

This report has URL
http://www.math.ntnu.no/preprint/numerics/2007/N11-2007.pdf
Address: Department of Mathematical Sciences, Norwegian University of Science and Technology, N-7491 Trondheim, Norway.

A Globally Convergent Numerical Method for Some Coefficient Inverse Problems With Resulting Second Order Elliptic Equations

Larisa Beilina[▽], Michael V. Klibanov[*]

December 18, 2007

A new globally convergent numerical method is developed for some multidimensional Coefficient Inverse Problems for hyperbolic and parabolic PDEs with applications in acoustics, electromagnetics and optical medical imaging. On each iterative step the Dirichlet boundary value problem for a second order elliptic equation is solved. The global convergence is rigorously proven and numerical experiments are presented.

1 Introduction

We present a new globally convergent numerical method for multidimensional Coefficient Inverse Problems (CIPs) for some hyperbolic and parabolic Partial Differential Equations (PDEs) with the data resulting from a single measurement event. The term "single measurement" means the boundary data obtained either from a single position of the point source or a single direction of the initializing plane wave. We describe this method, prove its convergence and present numerical results. In our definition "globally convergence" entails: (1) a rigorous convergence analysis that does not depend on the quality of the initial guess, and (2) numerical simulations that confirm the advertised convergence property.

The fundamental and commonly known obstacle for the development of numerical methods for CIPs is that residual least squares functionals are plagued by the phenomenon of multiple local minima and ravines. Therefore, any gradient-like minimization method for such a functional will likely converge to a wrong solution represented by a local minimum or even to almost any solution, in the case of a ravine. Furthermore, because of the ill-posedness, that functional might have many global minima, and there is no guarantee that any of them is close to the correct solution. Because of the above obstacle, conventional numerical methods for multidimensional CIPs, like, e.g., Newton-like methods, are locally convergent ones, see, e.g., [2, 3, 13, 27] and references cited there. This means that their convergence is rigorously guaranteed only if the starting point is located in a small neighborhood of the correct solution. However, in many applications a good initial guess is

[*▽] Larisa Beilina, NTNU, Department of Mathematical Science, 7491 Trondheim, Norway, *email*: Larisa.Beilina@math.ntnu.no

[*] Michael V. Klibanov, Department of Mathematics and Statistics University of North Carolina at Charlotte, Charlotte, NC 28223, USA, *email*: mklibanv@uncc.edu

unknown. The above means that solutions of multidimensional CIPs, provided by locally convergent methods, are fundamentally unreliable, see, e.g., [10] for a similar statement.

The development of globally convergent numerical methods for multidimensional CIPs has started recently from the so-called "convexification" algorithm [15, 17, 29]. The convexification is a globally convergent numerical method of the first generation. It uses a stable layer stripping procedure with respect to a spatial variable z and the projection method with respect to the rest of spatial variables. z-dependent Carleman Weight Functions (CWFs) are involved in the convexification. Because of this, the convexification can use boundary conditions only at one part of the boundary, i.e. at a side of a rectangular prism, which is orthogonal to z.

In this paper we develop a globally convergent numerical method for multidimensional CIPs of the second generation. It is *radically* different from the convexificiation. Unlike the convexification, the current method is not using neither the projection with respect to some spatial variables, nor the layer stripping with respect to a spatial variable. We use the layer stripping procedure with respect to the pseudo-frequency $s > 0$, where s the parameter of the Laplace transform of a hyperbolic/parabolic PDE. On each thin s-layer the Dirichlet boundary value problem for a nonlinear second order elliptic PDE is solved. This enables one to use the Dirichlet boundary condition at the entire boundary of the domain of interest. This condition in turn is the trace of the solution of the forward problem in a wider domain. s-dependent CWFs are present in our numerical scheme, which is one of essentially new elements here. This presence is important, because it enables one to weaken the influence of the nonlinear term in each of those elliptic PDEs on each s-layer, thus solving a linear problem on each iteration.

An important element of our method is a procedure of working with tails. We refer to section 4 of [27] for a similar treatment of tails for a locally convergent method. In [27] a layer stripping algorithm with respect to the source position x_0 running along a straight line was developed for an inverse problem for the equation $\Delta u - a(x) u = -\delta(x - x_0), x \in \mathbb{R}^3$ with the unknown coefficient $a(x)$.

Beginning from the remarkable paper of T. Carleman [9], weight functions carrying his name have been widely used for proofs of unique continuation and conditional stability results for ill-posed Cauchy problems for PDEs, as well as for multidimensional CIPs with the single measurement data, see, e.g. [16, 17, 20]. In this capacity CWFs were dependent on spatial variables, since they have provided weighted estimates for differential operators. However, CWFs of the current paper are used for integral Volterra-like operators, they are involved in the numerical scheme and depend on the pseudo frequency $s > 0$, rather than on a spatial variable. Since the Dirichlet boundary value problem is solved for each s-layer by the Finite Element Method (FEM), the method of this paper to rather general domains. We note that both the convexification and the current method are only general frameworks of corresponding specific algorithms. This means that each new specific CIP requires a major time consuming effort of re-programming of each of these methods, although within the same framework. Because of this, a straightforward numerical comparison of our current method with the convexification is outside of the scope of this publication. In our numerical experiments we image a medium with small inclusions in it, although we do not assume that the surrounding of inclusions is known. We refer to [1] and references cited there for another approach to imaging of small inclusions.

A substantially different layer stripping procedure with respect to the frequency (rather than pseudo frequency) was previously developed in [10], in which convergence theorem was not proven, however (remark 1.1 in [10]), and also CWFs were not used. The work [10] is treating the Fourier transform of the hyperbolic equation $c(x) u_{tt} = \Delta u$ with the unknown

coefficient $c(x)$. The iterative process of [10] starts from a low value of the frequency. Unlike this, we start from a high value of the pseudo frequency, because we can prove that by cutting off the high pseudo frequency range, which is commonly done in physics and engineering, we introduce only a small error. Unlike our technique, the method of [10] is not covering an important application to medical optical imaging. In the latter case the governing equation is $cu_t = \Delta u - a(x)u$, where $c = D^{-1}, D$ is the diffusion coefficient (usually $D \equiv const.$) and $a(x)$ is proportional to the absorption coefficient. The coefficient $a(x)$ is of the main interest in this application, see, e.g., the review paper [2].

There are also some other numerical methods for multidimensional CIPs, which do not require a good first guess. They are non-iterative ones, since they construct unknown coefficients via a series of steps. Unlike the current paper, they work for some CIPs with the data resulting from multiple measurements, rather than a single one. Because of multiple measurements, the applicability of these techniques is mostly limited to the over-determined CIPs, with the only exception of the 2-dimensional elliptic equation with a fixed frequency, which is non-over-determined. In computations the over-determination introduces an extra dimension, which is more expensive. We now cite only those methods, which are confirmed by published numerical results. Methods of [23], [24] and [22] were developed for CIPs for some elliptic equations with fixed frequency, and their numerical implementations in 2-D can be found respectively in [8] and [21]. Methods of [6] and [14] were developed for over-determined CIPs for some hyperbolic equations, and their numerical implementations can be found respectively in [7] and [14].

2 Statements of Forward and Inverse Problems

As forward problems, we consider Cauchy problems for some hyperbolic and parabolic PDEs. The case of a boundary value problem in a finite domain is not considered in our theoretical derivations only because an analogue of asymptotic behavior (2.12) is not proved in this case, since (2.12) is actually derived from Theorem 4.1 of [25]. That theorem establishes a certain asymptotic behavior of the fundamental solution of a hyperbolic equation near the characteristic cone. Consider the Cauchy problem for a hyperbolic equation

$$c(x)\, u_{tt} = \Delta u - a(x)u \text{ in } \mathbb{R}^3 \times (0, \infty), \tag{2.1}$$

$$u(x, 0) = 0, u_t(x, 0) = \delta(x - x_0). \tag{2.2}$$

In parallel, consider the Cauchy problem for a parabolic equation

$$c(x)\, \widetilde{u}_t = \Delta \widetilde{u} - a(x)\widetilde{u} \text{ in } \mathbb{R}^3 \times (0, \infty), \tag{2.3}$$

$$\widetilde{u}(x, 0) = \delta(x - x_0). \tag{2.4}$$

Equation (2.1) governs, e.g., propagation of acoustic and electromagnetic waves. In the acoustical case $1/\sqrt{c(x)}$ is the sound speed. In the case of EM waves propagation in a non-magnetic medium the dimensionless coefficient $c(x)$ is $c(x) = (\mu\epsilon)(x)$, where μ and ϵ are respectively the magnetic permeability and the electric permittivity of the medium. In the case of medical optical imaging, using propagation of the near infra red light, one uses parabolic equation (2.3), in which $c = D^{-1} = const > 0, D$ is the diffusion coefficient (usually the diffusion coefficient changes slowly in biological media) and $a(x) = c_l \mu_a(x)$, where $c_l = const.$ is the speed of light and $\mu_a(x)$ is the absorption coefficient of the medium, whose image is of an interest in this application, see, e.g., [2].

In principle, we can pose inverse problems for each of the equations (2.1) and (2.3) in the time domain. However, since our numerical method works with the Laplace transforms of

these equations, it is more convenient to pose inverse problems for the equation obtained by this transform. Statements in the time domain are similar. In the case of a finite time interval, on which measurements are performed, one should assume that this interval is large enough and thus, the t-integral of the Laplace transform over this interval is approximately the same as one over $(0,\infty)$. Consider the Laplace transforms of each of functions u and $\widetilde{u}$. We obtain

$$w(x,s)=\int\limits_0^\infty u(x,t)e^{-st}dt=\int\limits_0^\infty \widetilde{u}(x,t)e^{-s^2t}dt,\ \text{for } s>\underline{s}=const.>0, \tag{2.5}$$

where $\underline{s}$ is a certain number. In principle, it is sufficient to choose $\underline{s}$ such that integrals (2.5) would converge. However, we choose $\underline{s}$ experimentally in our numerical studies, because it is involved in our algorithm. We assume the positivity of the parameter s, because we need to make sure that the function $w(x,s)>0$ by the maximum principle. We call this parameter *pseudo frequency*.

As to the coefficients of equations (2.1) and (2.3), we assume that

$$c(x)\in(2d_1,2d_2),\ \text{where } d_1,d_2=const.>0. \tag{2.6}$$

$$c(x)\in C^2\left(\mathbb{R}^3\right),c(x)=c_0=const.\geq 2d_1 \text{ for } x\in\mathbb{R}^3\diagdown\Omega, \tag{2.7}$$

$$a(x)\in C^2\left(\mathbb{R}^3\right),a(x)\geq 0,a(x)=a_0=const.\geq 0 \text{ for } x\in\mathbb{R}^3\diagdown\Omega, \tag{2.8}$$

where $\Omega\subset\mathbb{R}^3$ is a bounded domain. The equation for the function w is

$$\Delta w-\left[s^2c(x)+a(x)\right]w=-\delta(x-x_0),\forall s\geq\underline{s}=const.>0. \tag{2.9}$$

Naturally, we impose the following condition at the infinity

$$\lim_{|x|\to\infty}w(x,s)=0,\forall s\geq\underline{s}=const.>0. \tag{2.10}$$

Condition (2.10) can be easily justified as follows. Classic estimates for the fundamental solution of the parabolic equation (2.3) actually estimate the function $\widetilde{u}(x,t)$ from the above via the solution of the same equation but with constant coefficients [18], Chapter 4, §13. Next, the Laplace transform for the latter solution can be calculated in a closed form and it satisfies (2.10). Using the classic technique for elliptic equations, one can prove that for every $s\geq\underline{s}$ there exists unique solution $w(x,s)\in C^3\left(\mathbb{R}^3\diagdown\{|x-x_0|<r\}\right),\forall r>0$ of the problem (2.9), (2.10). Furthermore, by the maximum principle

$$w(x,s)>0,\forall s\geq\underline{s}. \tag{2.11}$$

To justify the asymptotic behavior of the function $w(x,s)$ at $s\to\infty$, we need to formulate Lemma 2.1 [17].

Lemma 2.1. *Let the function $w(x,s)\in C^3\left(\mathbb{R}^3\diagdown\{|x-x_0|<\varepsilon\}\right),\forall\varepsilon>0$ be the solution of the problem (2.9), (2.10). Suppose that conditions (2.6)-(2.8) are satisfied. Assume that geodesic lines, generated by the eikonal equation corresponding to the function $c(x)$ are regular, i.e. any two points in $\mathbb{R}^3$ can be connected by a single geodesic line (this is true, of course, if $c\equiv const.>0$). Let $l(x,x_0)$ be the length of the geodesic line connecting points x and x_0. Then the following asymptotic behavior of the function w and its derivatives takes place for $|\alpha|\leq 2,\gamma=0,1,x\neq x_0$*

$$D_x^\alpha D_s^\gamma w(x,s)=D_x^\alpha D_s^\gamma\left\{\frac{\exp\left[-sl(x,x_0)\right]}{f(x,x_0)}\left[1+O\left(\frac{1}{s}\right)\right]\right\},s\to\infty, \tag{2.12}$$

where $f(x, x_0) > 0$ *is a certain sufficiently smooth function for* $x \neq x_0$.

Note that a certain over-smoothness of coefficients is usually assumed for a CIP. Actually, this is a certain consequence of the fundamental Tikhonov theorem [28]. This theorem claims the continuity on a compact set of an operator, which is an inverse to a one-to-one continuous operator. That compact set should be *a priori* known, because of *a priori* knowledge of the range of parameters for a specific applied inverse problem. In applications this compact set is often called the "set of admissible parameters". However, in our particular case, the C^2-smoothness required by Lemma 2.1 is also because of Theorem 4.1 of [25], which implies the asymptotic behavior (2.12). Note that Theorem 4.1 of [25] actually requires a higher smoothness of coefficients. This is because it is concerned with many terms of the asymptotic behavior of the fundamental solution of the hyperbolic equation near the characteristic cone. However, since (2.12) is dealing only with the first term of this behavior, then it follows from the proof of that theorem, that the C^2-smoothness is sufficient (also, see Acknowledgment). Still, we do not actually use the C^2-smoothness assumption in our computations. Instead we verify the asymptotic behavior (2.12) computationally, see subsection 7.3.

We formulate the inverse problem for the elliptic equation (2.9) with the condition (2.10).

Inverse Problem. Let $\Omega \subset \mathbb{R}^3$ be a convex bounded domain. Suppose that one of coefficients of the equation (2.9) is unknown in Ω, the other one is known, and both coefficients have known constant values outside of Ω. Determine that unknown coefficient for $x \in \Omega$, assuming that the following function $\varphi(x, s)$ is known for a single source position $x_0 \notin \overline{\Omega}$

$$w(x, s) = \varphi(x, s), \forall (x, s) \in \partial\Omega \times [\underline{s}, \overline{s}], \tag{2.13}$$

where $\overline{s} > \underline{s}$ is a number, which should be chosen experimentally in numerical studies.

The question of uniqueness of this Inverse Problem is a well known long standing open problem. However, in the case when the function $\delta(x - x_0)$ above is replaced with a "close" function $f(x) \neq 0, \forall x \in \overline{\Omega}$, it is addressed positively via the method of Carleman estimates, see, e.g., [16, 17]. It seems that such a replacement of the function $\delta(x - x_0)$ should not affect significantly the quality of numerical results, although we have not investigated this issue. It is an opinion of the authors that because of applications, it makes sense to develop numerical methods, assuming that the question of uniqueness of this problem is addressed positively. In addition, the question of uniqueness of the transformed equation (3.8) with the Cauchy data (3.9) was addressed positively, in Theorem 6.5.1 in [15] under the assumption that the function $V(x, \overline{s})$ is known.

3 Nonlinear Integral Differential Equation Without the Unknown Coefficient

Following one of ideas of the convexification, which actually has roots in the above mentioned method of Carleman estimates for CIPs [16, 15], we first transform our problem to the Cauchy problem for a nonlinear elliptic integral-differential equation, in which the unknown coefficient is not present. Because of (2.11), we can consider the function $v = \ln w$. Then (2.9) and (2.13) lead to

$$\Delta v + |\nabla v|^2 = s^2 c(x) + a(x) \text{ in } \Omega, \tag{3.1}$$

$$v(x, s) = \varphi_1(x, s), \ \forall (x, s) \in \partial\Omega \times [\underline{s}, \overline{s}], \tag{3.2}$$

where $\varphi_1 = \ln \varphi$. Consider, for example the case when the coefficient $c(x)$ is unknown. The idea is to eliminate $c(x)$ from equation (3.1) via the differentiation with respect to s, since $\partial_s c(x) = 0$. Introduce a new function $\widetilde{v}$ by

$$\widetilde{v} = \frac{v}{s^2}. \tag{3.3}$$

Assuming that conditions of Lemma 2.1 hold, we obtain

$$D_x^\alpha(\widetilde{v}) = O\left(\frac{1}{s}\right), D_x^\alpha D_s(\widetilde{v}) = O\left(\frac{1}{s^2}\right), s \to \infty. \tag{3.4}$$

By (3.1)

$$\Delta\widetilde{v} + s^2 (\nabla\widetilde{v})^2 = c(x) + s^{-2}a(x). \tag{3.5}$$

Denote

$$q(x,s) = \partial_s \widetilde{v}(x,s). \tag{3.6}$$

By (3.4) and (3.6)

$$\widetilde{v}(x,s) = -\int_s^\infty q(x,\tau)\, d\tau.$$

We truncate this integral as

$$\widetilde{v}(x,s) \approx -\int_s^{\overline{s}} q(x,\tau)\, d\tau + V(x,\overline{s}), \tag{3.7}$$

where $\overline{s} > s_0$ is a large number which should be chosen in numerical experiments, see subsection 6.3 for some discussion. We call the function $V(x,\overline{s})$ in (3.7) the "tail", and this function is unknown. By (3.4) the tail is small for the large values of $\overline{s}$. In principle, therefore, one can set $V(x,\overline{s}) := 0$. However, our numerical experience, as well as section 4 of [27], show that it would be better to somehow approximate the tail function via updating it in an iterative procedure, and we describe this procedure in section 5. We call this procedure "iterations with respect to tails".

Below we set $a(x) := 0$ for brevity. We note that in the case when the coefficient $a(x)$ is unknown, rather than $c(x)$, one should replace functions v and q above with

$$\widehat{v} = v + sl(x,x_0), \widehat{q}(x,s) = \partial_s v + l(x,x_0),$$

which will guarantee a direct analogue of the proper asymptotic behavior (3.4). The rest of the method of this article will remain almost the same with a few insignificant changes.

Thus, we obtain from (3.5)-(3.7) the following (approximate) integral nonlinear differential equation

$$\Delta q - 2s^2 \nabla q \cdot \int_s^{\overline{s}} \nabla q(x,\tau)\, d\tau + 2s\left[\int_s^{\overline{s}} \nabla q(x,\tau)\, d\tau\right]^2 \tag{3.8}$$

$$+2s^2 \nabla q \nabla V - 2s\nabla V \cdot \int_s^{\overline{s}} \nabla q(x,\tau)\, d\tau + 2s(\nabla V)^2 = 0$$

In addition, (3.2), (3.3) and (3.6) imply that the following Dirichlet boundary condition is given for the function q

$$q(x,s) = \psi(x,s), \ \forall (x,s) \in \partial\Omega \times [\underline{s}, \overline{s}], \tag{3.9}$$

where

$$\psi(x,s) = \frac{1}{s^2\varphi} \cdot \frac{\partial \varphi}{\partial s} - \frac{2\ln\varphi}{s^3}.$$

Suppose for a moment that the function q is approximated together with its derivatives $D_x^\alpha q, |\alpha| \leq 2$. Then a corresponding approximation for the target coefficient can be found via (3.4) as

$$c(x) = \Delta\widetilde{v} + \underline{s}^2 (\nabla\widetilde{v})^2, \tag{3.10}$$

where the function $\widetilde{v}$ is found from (3.4). Although any value of the pseudo frequency $s \in [\underline{s}, \overline{s}]$ can be used in (3.10), but we found in our numerical experiments that the best value is $s := \underline{s}$. An equation, similar with (3.8), was previously derived in the convexification method [15], although with both Dirichlet and Neumann data given only at a part of $\partial\Omega$. Regardless on the difference in the data setting, the *major* difference between the current method and the convexification is in the procedure of solving equation (3.8). Indeed, (3.8) is a nonlinear elliptic integral differential equation, in which the integration is carried out with respect to a parameter, which is not involved in the differential operator. If integrals would be absent and the tail function would be known, then this would be a simple Dirichlet boundary value problem for the Poisson equation. However, the presence of integrals implies the nonlinearity, which is the main difficulty here. Thus, below we are mostly concerned with the following question: *How to solve numerically the problem (3.8), (3.9)?*

4 Layer Stripping With Respect to the Pseudo Frequency

We approximate the function $q(x,s)$ as a piecewise constant function with respect to the pseudo frequency s. That is, we assume that there exists a partition

$$\underline{s} = s_N < s_{N-1} < ... < s_1 < s_0 = \overline{s}, s_{i-1} - s_i = h$$

of the interval $[\underline{s}, \overline{s}]$ with sufficiently small grid step size h such that

$$q(x,s) = q_n(x) \ \text{ for } s \in (s_n, s_{n-1}].$$

Hence

$$\int_s^{\overline{s}} \nabla q(x,\tau)\, d\tau = (s_{n-1} - s)\nabla q_n(x) + h\sum_{j=1}^{n-1} \nabla q_j(x), s \in (s_n, s_{n-1}]. \tag{4.1}$$

We approximate the boundary condition (3.9) as a piecewise constant function,

$$q_n(x) = \overline{\psi}_n(x), x \in \partial\Omega, \tag{4.2}$$

where

$$\overline{\psi}_n(x) = \frac{1}{h}\int_{s_n}^{s_{n-1}} \psi(x,s)\, ds. \tag{4.3}$$

Hence, equation (3.8) can be rewritten as

$$\widetilde{L}_n(q_n) := \Delta q_n - 2\left(s^2 - 2s(s_{n-1}-s)\right)\left(h\sum_{j=1}^{n-1}\nabla q_j(x)\right)\cdot\nabla q_n$$

$$+2\left(s^2 - 2s(s_{n-1}-s)\right)\nabla q_n\cdot\nabla V(x,\overline{s})$$

$$= 2(s_{n-1}-s)\left[s^2 - s(s_{n-1}-s)\right](\nabla q_n)^2 - 2sh^2\left(\sum_{j=1}^{n-1}\nabla q_j(x)\right)^2 \tag{4.4}$$

$$+4s\nabla V(x,\overline{s})\cdot\left(h\sum_{j=1}^{n-1}\nabla q_j(x)\right) - 2s\left[\nabla V(x,\overline{s})\right]^2, s\in(s_{n-1},s_n]$$

Equation (4.4) is nonlinear and it depends on the parameter s, whereas the function $q_n(x)$ is independent on s. This discrepancy is due to the approximation of the function $q(x,s)$ by a piecewise constant function. Although it seems that equation (4.4) is over-determined because the function $q_n(x)$ is not changing withe the change of s, but variations of s-dependent coefficients of (4.4) are small over $s\in[s_n,s_{n-1})$, because this interval is small. This discrepancy is helpful for the method, because it enables us to "mitigate" the influence of the nonlinear term $(\nabla q_n)^2$ in (4.4) via introducing the s-dependent CWF.

In addition, we add the term $-\varepsilon q_n$ to the left hand side of equation (4.4), where $\varepsilon>0$ is a small parameter. We are doing this because, by the maximum principle, if a function $p(x,s)$ is the classical solution of the Dirichlet boundary value problem

$$\widetilde{L}_n(p) - \varepsilon p = f(x,s) \text{ in } \Omega, p\mid_{\partial\Omega} = p_b(x,s),$$

then [19] (Chapter 3, §1)

$$\max_{\overline{\Omega}}|p| \le \max\left[\max_{\partial\Omega}|p_b|, \varepsilon^{-1}\max_{\overline{\Omega}}|f|\right], \forall s\in(s_{n-1},s_n]. \tag{4.5}$$

On the other hand, if $\varepsilon=0$, then the analogous estimate would be worse because of the involvement of some constants depending on $\max_{\overline{\Omega}}|\nabla q_j|$. Therefore, it is anticipated that the introduction of the term $-\varepsilon q_n$ should provide a better stability of our process, and we indeed observe this in our computations (subsection 7.3).

Introduce the s-dependent Carleman Weight Function $\mathcal{C}_{n\lambda}(s)$ by

$$\mathcal{C}_{n\mu}(s) = \exp\left[-\lambda|s-s_{n-1}|\right], s\in(s_n,s_{n-1}], \tag{4.6}$$

where $\lambda >> 1$ is a parameter. In real computations this parameter should be chosen experimentally (subsection 7.3). Theorem 6.1 establishes that it is possible to choose an appropriate value of λ, and the proof of this theorem provides a recipe for such a choice. Multiply both sides of (4.4) by this CWF and integrate with respect to s over the interval $[s_n,s_{n-1}]$. We obtain

$$L_n(q_n) := \Delta q_n - A_{1,n}\left(h\sum_{i=1}^{n-1}\nabla q_i\right)\cdot\nabla q_n + A_{1n}\nabla q_n\cdot\nabla V - \varepsilon q_n$$

$$= 2\frac{I_{1,n}}{I_0}(\nabla q_n)^2 - A_{2,n}h^2\left(\sum_{i=1}^{n-1}\nabla q_i(x)\right)^2 \tag{4.7}$$

$$+2A_{1,n}\nabla V\cdot\left(h\sum_{i=1}^{n-1}\nabla q_i\right)-A_{2,n}\left(\nabla V\right)^2,$$

where

$$I_0:=I_0\left(\lambda,h\right)=\int\limits_{s_{n-1}}^{s_n}\mathcal{C}_{n\lambda}\left(s\right)ds=\frac{1-e^{-\lambda h}}{\lambda},$$

$$I_{1,n}:=I_{1,n}\left(\lambda,h\right)=\int\limits_{s_{n-1}}^{s_n}\left(s_{n-1}-s\right)\left[s^2-s\left(s_{n-1}-s\right)\right]\mathcal{C}_{n\lambda}\left(s\right)ds,$$

$$A_{1,n}:=A_{1,n}\left(\lambda,h\right)=\frac{2}{I_0}\int\limits_{s_{n-1}}^{s_n}\left(s^2-2s\left(s_{n-1}-s\right)\right)\mathcal{C}_{n\lambda}\left(s\right)ds,$$

$$A_{2,n}:=A_{2,n}\left(\lambda,h\right)=\frac{2}{I_0}\int\limits_{s_{n-1}}^{s_n}s\mathcal{C}_{n\lambda}\left(s\right)ds.$$

An important observation is that

$$\frac{\left|I_{1,n}\left(\lambda,h\right)\right|}{I_0\left(\lambda,h\right)}\leq\frac{C}{\lambda},\text{ for }\lambda h\geq 1, \tag{4.8}$$

where $C>0$ is an absolute constant independent on λ,h,n. Therefore, by taking $\lambda>>1$, we mitigate the influence of the nonlinear term with $\left(\nabla q_n\right)^2$ in (4.6), and we use this in our iterative algorithm via solving a linear problem on each iterative step.

Remark 4.1. In computations the above integrals with the CWF should be calculated in closed forms. This is because for large λ the function $\mathcal{C}_{n\lambda}\left(s\right)$ is changing rapidly and, therefore, the integration step size should be taken too small. In principle, one can decrease the step size h in the s-direction instead of using the CWF. However, the introduction of the CWF provides more flexibility for the choice of parameters for computations, since parameters h and λ are independent, as long as $\lambda h\geq 1$. In addition, taking h too small would increase of the computational time, because one would need to compute sequentially too many functions q_n. Finally, our computational experience shows that one should choose different parameters $\lambda:=\lambda_n$ for different values of n, see subsection 7.3. Hence, the absence of CWFs would mean the choice of a variable step size h, which would only introduce additional complications in the algorithm.

5 The Algorithm

The above considerations lead to the algorithm described in this section. Below $C^{k+\alpha}\left(\overline{\Omega}\right)$ are Hőlder spaces, where $k\geq 0$ is an integer and $\alpha\in(0,1)$ [19]. In particular, we describe here an important procedure for updating tails, which we call "iterations with respect to tails". In our numerical experiments the starting value for tails $V_{1,1}:=0$, which corresponds well with the asymptotic behavior (3.4) and also reflects the fact that we do not have a good first guess about the solution. In the convergence theorem we assume that $\left\|V_{1,1}\right\|_{C^{2+\alpha}\left(\overline{\Omega}\right)}$ is sufficiently small.

Since in an applied scenario the boundary data for an inverse problem are given from real measurements, then one does not need to solve the forward problem in this cas to

generate the data. In our case, however, we first need to generate the data from the solution of the forward problem (2.1), (2.2) and to work with the boundary data (4.2) then, pretending that we have "forgotten" about the coefficient $c(x)$, as it is always done in computational simulations for inverse problems. Hence, we assume in this section that the forward problem is already solved and the data (4.2) are generated. We assume in this and next sections that $\Omega \subset \mathbb{R}^3$ is a convex bounded domain and $\partial\Omega \in C^3$.

Remark 5.1. Note that we need $\mathbb{R}^3$ rather than $\mathbb{R}^2$ in our derivations only to justify the asymptotic behavior (3.4), because of Lemma 2.1. However, if assuming that such a behavior holds, then we can consider both $\mathbb{R}^3$ and $\mathbb{R}^2$. In our numerical experiments, which are in 2-D, we verify this asymptotic behavior computationally.

Remark 5.2. In our algorithm we reconstruct iterative approximations $c_{n,k}(x) \in C^{\alpha}\left(\overline{\Omega}\right)$ only inside the domain Ω. On the other hand, to iterate with respect to tails, we need to solve the forward problem (2.9), (2.10) in the entire space $\mathbb{R}^3$ with $c(x) := c_{n,k}(x)$ and $a(x) = 0$. To do so, we need to extend each function $c_{n,k}(x)$ outside of the domain Ω in such a way that the resulting function $\widehat{c}_{n,k} \in C^{\alpha}\left(\mathbb{R}^3\right)$ and $\widehat{c}_{n,k} = 2d_1$ outside of Ω. This can be done in a standard way via considering a bigger "transitional" convex bounded domain $\Omega' \supset \Omega$ and using such a function $\chi(x) \in C^1\left(\mathbb{R}^3\right)$ that

$$\chi(x) = \left\{ \begin{array}{c} 1 \text{ in } \Omega, \\ \text{between 1 and } 2d_1 \text{ in } \Omega' \diagdown \Omega, \\ 2d_1 \text{ outside of } \Omega'. \end{array} \right\}.$$

The existence of such functions $\chi(x)$ is well known from the Real Analysis course. The resulting function in this case is $\chi(x) c_{n,k}(x) := \widehat{c}_{n,k}(x) \in C^{\alpha}\left(\mathbb{R}^3\right)$ and $\widehat{c}_{n,k}(x) = const. = 2d_1$ outside of Ω'. So, everywhere below we assume without further mentioning that this procedure is applied to each function $c_{n,k}(x)$. In our numerical experiments we simply extend each function $c_{n,k}(x)$ outside of our specific domain Ω as $\widehat{c}_{n,k}(x) = 1$. This is because our correct target function equals 1 near the boundary of Ω.

Step 1^1. Choose an initial tail function $V_{1,1}(x, \overline{s}) \in C^{2+\alpha}\left(\overline{\Omega}\right)$. Choose a large parameter $\lambda >> 1$ and a small parameter $\varepsilon \in (0,1)$. To compute the first approximation $q_{1,1}$ for the function q_1 for this tail, solve the following Dirichlet boundary value problem

$$\Delta q_{1,1} + A_{1,1} \nabla q_{1,1} \cdot \nabla V_{1,1} - \varepsilon q_{1,1} = -A_{2,1} \left(\nabla V_{1,1}\right)^2, \tag{5.1}$$

$$q_{1,1} = \overline{\psi}_1(x), x \in \partial\Omega, \tag{5.2}$$

By the Schauder's theorem (see beginning of subsection 6.2) the problem (5.1), (5.2) has unique solution $q_{1,1} \in C^{2+\alpha}\left(\overline{\Omega}\right)$. Reconstruct an approximation $c_{1,1}(x) \in C^{\alpha}\left(\overline{\Omega}\right)$ for the unknown coefficient $c(x)$ using the function $q_{1,1}(x)$ and formulas (3.7), (3.10) with $V(x, \overline{s}) := V_{1,1}(x, \overline{s})$, $\underline{s} := s_1$.

Step 1^k, $k \geq 2$. Solve the forward problem (2.9), (2.10), in which $c(x) := c_{1,k-1}(x)$, $a(x) = 0, s = \overline{s}$. We obtain the function $w_{1,k}(x, \overline{s})$ this way. Update the tail function as

$$V_{1,k}(x, \overline{s}) = \frac{1}{\overline{s}^2} \ln w_{1,k}(x, \overline{s}) \in C^{2+\alpha}\left(\overline{\Omega}\right). \tag{5.3}$$

Next, solve the boundary value problem for equation

$$\Delta q_{1,k} + A_{1,1} \nabla q_{1,k} \cdot \nabla V_{1,k} - \varepsilon q_{1,k} = 2\frac{I_{1,1}}{I_0} \left(\nabla q_{1,k-1}\right)^2 - A_{2,1} \left(\nabla V_{1,k}\right)^2 \tag{5.4}$$

with the boundary condition (4.2) (at $n = 1$). We obtain the function $q_{1,k} \in C^{2+\alpha}\left(\overline{\Omega}\right)$. Reconstruct a new approximation $c_{1,k} \in C^{\alpha}\left(\overline{\Omega}\right)$ for the unknown coefficient using the function $q_{1,k}(x)$ and formulas (3.7), (3.10) with

$V(x,\overline{s}) := V_{1,k}(x,\overline{s}), \underline{s} := s_1$. Make several steps $1^1, 1^2, .., 1^{m_1}$. As a result, we obtain functions $q_1 \in C^{2+\alpha}\left(\overline{\Omega}\right), c_1 \in C^{\alpha}\left(\overline{\Omega}\right)$, where

$$q_1(x) := q_{1,m_1}(x), c_1(x) := c_{1,m_1}(x). \tag{5.5}$$

Step n^1. Having functions $q_1, ..., q_{n-1} \in C^{2+\alpha}\left(\overline{\Omega}\right)$ and the tail function $V_{n-1,m_{n-1}}(x,\overline{s}) \in C^{2+\alpha}\left(\overline{\Omega}\right)$, set

$$V_{n,1}(x,\overline{s}) := V_{n-1,m_{n-1}}(x,\overline{s}), \tag{5.6}$$

$$q_{n,0} := q_{n-1}. \tag{5.7}$$

Solve the following elliptic boundary value problem for the function $q_{n,1}$

$$\Delta q_{n,1} - A_{1n}\left(h\sum_{j=1}^{n-1}\nabla q_j\right)\cdot\nabla q_{n,1} - \varepsilon q_{n,1} + A_{1,n}\nabla q_{n,k}\cdot\nabla V_{n,1} =$$

$$2\frac{I_{1,n}}{I_0}\left(\nabla q_{n,0}\right)^2 - A_{2,n}h^2\left(\sum_{j=1}^{n-1}\nabla q_j(x)\right)^2 \tag{5.8}$$

$$+2A_{2,n}\nabla V_{n,1}\cdot\left(h\sum_{j=1}^{n-1}\nabla q_j(x)\right) - A_{2,n}\left(\nabla V_{n,1}\right)^2,$$

$$q_{n,1}(x) = \overline{\psi}_n(x), x \in \partial\Omega. \tag{5.9}$$

Hence, we obtain the function $q_{n,1} \in C^{2+\alpha}\left(\overline{\Omega}\right)$. Reconstruct an approximation $c_{n,1}(x) \in C^{\alpha}\left(\overline{\Omega}\right)$ for the unknown $c(x)$ using the function $q_{n,1}(x)$, as well as functions $q_1, ..., q_{n-1}$ and formulas (3.7), (3.10), where $V(x,\overline{s}) := V_{n,1}(x,\overline{s}), \underline{s} := s_n$.

Step n^k, $k \geq 2$. Solve the forward problem (2.9), (2.10), in which $c(x) := c_{n,k-1}(x)$, $a(x) = 0, s = \overline{s}$. We obtain the function $w_{n,k}(x,\overline{s})$ this way. Update the tail function as

$$V_{n,k}(x,\overline{s}) = \frac{1}{\overline{s}^2}\ln w_{n,k}(x,\overline{s}) \in C^{2+\alpha}\left(\overline{\Omega}\right). \tag{5.10}$$

Next, solve the boundary value problem

$$\Delta q_{n,k} - A_{1,n}\left(h\sum_{j=1}^{n-1}\nabla q_j\right)\cdot\nabla q_{n,k} - \varepsilon q_{n,k} + A_{1,n}\nabla q_{n,k}\cdot\nabla V_{n,k}$$

$$= 2\frac{I_{1n}}{I_0}\left(\nabla q_{n,k-1}\right)^2 - A_{2,n}h^2\left(\sum_{j=1}^{n-1}\nabla q_j(x)\right)^2 \tag{5.11}$$

$$+2A_{2,n}\nabla V_{n,k}\cdot\left(h\sum_{j=1}^{n-1}\nabla q_j(x)\right) - A_{2,n}\left(\nabla V_{n,k}\right)^2,$$

$$q_{n,k}(x) = \overline{\psi}_n(x), x \in \partial\Omega \tag{5.12}$$

Reconstruct a new approximation $c_{n,k}(x)$ for the unknown coefficient, using (3.7) and (3.10) with $V(x,\overline{s}) := V_{n,k}(x,\overline{s}), \underline{s} := s_n$. Make several steps $n^1, n^2, .., n^{m_n}$. As a result, we obtain the following functions

$$q_n := q_{n,m_n} \in C^{2+\alpha}\left(\overline{\Omega}\right), c_n := c_{n,m_n} \in C^{\alpha}\left(\overline{\Omega}\right). \tag{5.13}$$

If the functions $c_n(x)$ did not yet converge, then proceed with Step $(n+1)^1$, provided that $n < N$. However, if either functions $c_n(x)$ converged, or $n = N$, then stop.

6 Global Convergence Theorem

Below we follow the concept of Tikhonov for ill-posed problems [28], which is one of backbones of this theory. By this concept, one should assume first that there exists an "ideal" exact solution of the problem with the exact data. Next, one should assume the presence of an error in the data of the level ζ, where $\zeta > 0$ is a small parameter. Suppose that an approximate solution is constructed for each sufficiently small ζ. This solution is called a "regularized solution", if the $\zeta-$dependent family of these solutions tends to the exact solution as ζ tends to zero. Hence, one should prove this convergence (Theorem 6.1).

6.1 Exact solution

First, we introduce the definition of the exact solution. We assume that there exists an exact coefficient function $c^*(x) \in C^\alpha\left(\overline{\Omega}\right)$, $\alpha = const. \in (0,1)$, which is a solution of our Inverse Problem. Let the function

$$w^*(x,s) \in C^{2+\alpha}\left(\mathbb{R}^3 \diagdown \{|x-x_0| < \eta\}\right), \forall \eta > 0, \forall s > \underline{s}$$

be the solution of the problem (2.9), (2.10) with $c(x) := c^*(x)$. Also, let

$$\widetilde{v}^*(x,s) = \frac{\ln[w^*(x,s)]}{s^2},\ q^*(x,s) = \frac{\partial \widetilde{v}^*(x,s)}{\partial s},\ V^*(x,\overline{s}) = \widetilde{v}^*(x,\overline{s}).$$

By (3.10)

$$c^*(x) = \Delta \widetilde{v}^* + \underline{s}^2 (\nabla \widetilde{v}^*)^2. \tag{6.1}$$

Also, the function q^* satisfies the following analogue of equation (3.8)

$$\Delta q^* - 2s^2 \nabla q^* \cdot \int\limits_s^{\overline{s}} \nabla q^*(x,\tau)\, d\tau + 2s \left[\int\limits_s^{\overline{s}} \nabla q^*(x,\tau)\, d\tau\right]^2 \tag{6.2}$$

$$+2s^2 \nabla q^* \nabla V^* - 2s \nabla V^* \cdot \int\limits_s^{\overline{s}} \nabla q^*(x,\tau)\, d\tau + 2s (\nabla V^*)^2 = 0, (x,s) \in \Omega \times [\underline{s}, \overline{s}],$$

with the boundary condition (see (3.9))

$$q^*(x,s) = \psi^*(x,s), (x,s) \in \partial\Omega \times [\underline{s}, \overline{s}], \tag{6.3}$$

where by (2.13)

$$\psi^*(x,s) = \frac{1}{\varphi^* s^2} \cdot \frac{\partial \varphi^*}{\partial s} - \frac{2 \ln \varphi^*}{s^3},$$

where $\varphi^*(x,s) = w^*(x,s)\,|_{x \in \partial\Omega}$.

Definition. We call the function $q^*(x,s)$ *the exact solution* of the problem (3.8), (3.9) with the *exact boundary* condition $\psi^*(x,s)$. Naturally, the function $c^*(x)$ from (6.1) is called the *exact solution* of our Inverse Problem.

Therefore,

$$q^*(x,s) \in C^{2+\alpha}\left(\overline{\Omega}\right) \times C^\infty[\underline{s}, \overline{s}]. \tag{6.4}$$

We now approximate the function $q^*(x,s)$ via a piecewise constant function with respect to $s \in [\underline{s}, \overline{s}]$. Let

$$q_n^*(x) = \frac{1}{h} \int\limits_{s_n}^{s_{n-1}} q^*(x,s)\, ds,\ \psi_n^*(x) = \frac{1}{h} \int\limits_{s_n}^{s_{n-1}} \psi^*(x,s)\, ds$$

Then

$$q^*(x,s) = q_n^*(x) + Q_n(x,s), \psi^*(x,s) = \psi_n^*(x) + \Psi_n(x,s), s \in [s_n, s_{n-1}], \tag{6.5}$$

where by (6.4) functions Q_n, Ψ_n are such that for $s \in [s_n, s_{n-1}]$

$$\|Q_n(x,s)\|_{C^{2+\alpha}(\overline{\Omega})} \leq C^* h, \|\Psi_n(x,s)\|_{C^{2+\alpha}(\overline{\Omega})} \leq C^* h, n = 1, ..., N, \tag{6.6}$$

where the constant $C^* > 0$ depends only on $C^{2+\alpha}\left(\overline{\Omega}\right) \times C^1[\underline{s}, \overline{s}]$ and $C^{2+\alpha}(\partial\Omega) \times C^1[\underline{s}, \overline{s}]$ norms of functions q^* and ψ^* respectively. Hence,

$$q_n^*(x) = \overline{\psi}_n^*(x), x \in \partial\Omega \tag{6.7}$$

and the following analogue of equation (4.7) holds

$$\begin{aligned} &\Delta q_n^* - A_{1,n}\left(h\sum_{i=1}^{n-1}\nabla q_i^*(x)\right)\cdot\nabla q_n^* + A_{1,n}\nabla q_n^*\cdot\nabla V^*(x,\overline{s}) \\ &= 2\frac{I_{1,n}}{I_0}(\nabla q_n^*)^2 - A_{2,n}h^2\left(\sum_{i=1}^{n-1}\nabla q_i^*(x)\right)^2 \\ &+2A_{2,n}h\nabla V^*(x,\overline{s})\cdot\left(h\sum_{i=1}^{n-1}\nabla q_i^*(x)\right) - A_{2,n}\left[\nabla V^*(x,\overline{s})\right]^2 + F_n(x,h,\lambda), \end{aligned} \tag{6.8}$$

where the function $F_n(x,h,\lambda) \in C^\alpha\left(\overline{\Omega}\right)$ and

$$\max_{\mu h \geq 1}\|F_n(x,h,\lambda)\|_{C^\alpha(\overline{\Omega})} \leq C^* h. \tag{6.9}$$

We also assume that the data $\varphi(x,s)$ in (2.13) are given with an error. This naturally produces an error in the function $\psi(x,s)$ in (3.9). An additional error is introduced due to the averaging in (4.3). Hence, it is reasonable to assume that

$$\left\|\overline{\psi}_n^*(x) - \overline{\psi}_n(x)\right\|_{C^{2+\alpha}(\partial\Omega)} \leq C_1(\sigma + h), \tag{6.10}$$

where $\sigma > 0$ is a small parameter characterizing the level of the error in the data $\psi(x,s)$, and the constant $C_1 > 0$ is independent on numbers σ, h and n.

Remark 6.1. It should be noted that usually the data $\varphi(x,s)$ in (2.13) are given with a random noise and the differentiation of the noisy data is an ill-posed problem, see section 7 for our way of handling it.

6.2 Convergence theorem

First, we reformulate the Schauder's theorem in a way, which is convenient for our case, see [26], and Chapter 3, §1 in [19] for this theorem. Denote

$$B = \max_{1\leq n\leq N}\left[2, \max_{\lambda h \geq 1}\left(A_{1,n}(\lambda,h), A_{2,n}(\lambda,h)\right)\right].$$

Introduce the positive constant M^* by

$$M^* = B\left\{\left[\max_{1\leq n\leq N}\left(\|q_n^*\|_{C^{1+\alpha}(\overline{\Omega})}\right) + \|V^*\|_{C^{1+\alpha}(\overline{\Omega})} + 1\right], 2C, C^*, C_1\right\},$$

where C and C^* are constants from (4.8), (6.9) and (6.10) respectively. Since the constant B depends on $\overline{s}$ and $\underline{s}$, then

$$M^* = M^* \left(\max_{1 \leq n \leq N} \|q_n^*\|_{C^{1+\alpha}(\overline{\Omega})}, \|V^*\|_{C^{1+\alpha}(\overline{\Omega})}, \underline{s}, \overline{s} \right).$$

Consider the Dirichlet boundary value problem

$$\Delta u + \sum_{j=1}^{3} b_j(x) u_{x_j} - d(x) u = f(x), \; x \in \Omega,$$

$$u \mid_{\partial\Omega} = g(x) \in C^{2+\alpha}(\partial\Omega),$$

where functions

$$b_j, d, f \in C^{\alpha}\left(\overline{\Omega}\right), d(x) \geq 0; \;\; \max\left(\|b_j\|_{C^{\alpha}(\overline{\Omega})}, \|d\|_{C^{\alpha}(\overline{\Omega})} \right) \leq M^*.$$

By the Schauder theorem there exists unique solution $u \in C^{2+\alpha}\left(\overline{\Omega}\right)$ of this problem and with a constant $K = K(M^*, \Omega) > 0$ the following estimate holds

$$\|u\|_{C^{2+\alpha}(\overline{\Omega})} \leq K \left[\|g\|_{C^{2+\alpha}(\partial\Omega)} + \|f\|_{C^{\alpha}(\overline{\Omega})} \right].$$

Theorem 6.1. *Let $\Omega \subset \mathbb{R}^3$ be a convex bounded domain with the boundary $\partial\Omega \in C^3$. Let the exact coefficient $c^* \in C^2\left(\mathbb{R}^3\right)$, $c^* \in (2d_1, 2d_2)$ and $c^*(x) = const. \geq 2d_1$ for $x \in \mathbb{R}^3 \setminus \Omega$. For any function $c(x) \in C^{\alpha}\left(\mathbb{R}^3\right)$ such that $c(x) \geq d_1$, $c(x) = 2d_1$ for $x \in R^3 \setminus \Omega$ consider the solution $w_c(x, \overline{s}) \in C^3\left(\mathbb{R}^3 \setminus \{|x - x_0| < r\}\right), \forall r > 0$ of the problem (2.9), (2.10) with $a(x) = 0$. Let $V_c = \overline{s}^{-2} \ln w_c(x, \overline{s}) \in C^{2+\alpha}\left(\overline{\Omega}\right)$ be the corresponding tail function. Suppose that the cut-off pseudo frequency $\overline{s}$ is so large that for any such function $c(x)$ satisfying the inequality $\|c - c^*\|_{C^{\alpha}(\overline{\Omega})} \leq d_1$ the following estimates hold*

$$\|V^*\|_{C^{2+\alpha}(\overline{\Omega})} \leq \xi, \|V_c\|_{C^{2+\alpha}(\overline{\Omega})} \leq \xi, \tag{6.11}$$

where $\xi \in (0,1)$ is a sufficiently small number. Let $V_{1,1}(x, \overline{s}) \in C^{2+\alpha}\left(\overline{\Omega}\right)$ be the initial tail function and let

$$\|V_{1,1}\|_{C^{2+\alpha}(\overline{\Omega})} \leq \xi. \tag{6.12}$$

Denote $\eta = h + \sigma + \xi + \varepsilon$. Let $\overline{N} \leq N$ be the total number of functions q_n calculated by the above algorithm. Suppose that the number $\overline{N} = \overline{N}(h)$ is connected with the step size h via $\overline{N}(h) h = \beta$, where the constant $\beta > 0$ is independent on h. Let β be so small that

$$\beta \leq \min\left(\frac{1}{2M^*}, \frac{1}{16KM^*} \right). \tag{6.13}$$

Then there exists a sufficiently small number $\eta_0 = \eta_0(K(M^*, \Omega), M^*, \underline{s}, \overline{s}, d_1, d_2) \in (0,1)$ and a sufficiently large number $\lambda = \lambda(K(M^*, \Omega), M^*, \eta) > 1$ such that for all $\eta \in (0, \eta_0)$ and for every integer $n \in \left[1, \overline{N}\right]$ the following estimates hold

$$\|q_n - q_n^*\|_{C^{2+\alpha}(\overline{\Omega})} \leq 2KM^* \left(\frac{1}{\sqrt{\lambda}} + 3\eta \right), \tag{6.14}$$

$$\|q_n\|_{C^{2+\alpha}(\overline{\Omega})} \leq 2M^*, \tag{6.15}$$

$$\|c_n - c^*\|_{C^\alpha(\overline{\Omega})} \leq 10K\left(M^*\right)^2\left(1+\overline{s}^2\right)\left(\frac{1}{\sqrt{\lambda}}+3\eta\right). \tag{6.16}$$

Remarks 6.2:

1. The parameter η characterizes the error both in the data and in our mathematical model. One should have $\eta \to 0$. However, since in the reality it is off its limiting value and we also have some other parameters, it is important to conduct numerical experiments, which would verify this theorem.

2. Truncating integrals at a high pseudo frequency $\overline{s}$ is a natural thing to do, because in physics and engineering one routinely truncates high frequencies. By truncating integrals, we actually come up with a different, although a quite reasonable mathematical model. Consider now the influence of this truncation on the accuracy of the reconstruction. Let, for example $h = \varepsilon = \sigma = \xi$, and $\lambda^{-1/2} = \xi$. Then estimates (6.14)-(6.16) imply that the error of our reconstruction is $O(\xi)$ for $\xi \to 0$. In other words, one of claims of Theorem 6.1 is that the error of the reconstruction of the unknown coefficient is mainly determined by the truncation error, which means the error in our new mathematical model. This conclusion is going along well with our numerical experiments, see subsection 7.4.

3. Conditions (6.11), (6.12) with a small number ξ are natural ones, because the number $\overline{s}$ is supposed to be sufficiently large, and by (3.4) the function $\widetilde{v}(x,\overline{s})$ tends to zero together with its x-derivatives as $\overline{s} \to \infty$. Therefore, the condition (6.12) *does not* imply the assumption of the closedness of the first guess to the correct solution. For example, one can simply choose the initial tail function $V_{1,1} = 0$, which we do numerically, and (6.12) would still hold for a large $\overline{s}$.

4. One of basic ideas of the theory of ill-posed problems is that the number of iterations can be chosen as a regularization parameter, see, e.g., page 157 of [11]. In principle, therefore, we have a vector $\left(\overline{N}, m_1, ..., m_{\overline{N}}\right)$ of regularization parameters. However, we work in a simpler way in our computations: we take in our computations $m_1 = m_2 = ... = m_{n_0} = 4$ up to a certain number n_0 and then we take $m_{n_0+1} = m_{n_0+2} = ... = m_{\overline{N}} = 7$, see details in subsection 7.3. Setting $\overline{N}(h)\, h = \beta = const. > 0$ is in an agreement with, e.g.,, Lemma 6.2 on page 156 of [11], since this lemma shows a connection between the error in the data and the number of iterations (that lemma is proven for a different algorithm). In our case h can be considered as a part of the error in the data, since we have replaced a smooth s-dependent function with a piecewise constant one. In our computations $h = 0.05$, $\overline{N} \leq 12$, and $N = 15$. The fact that in some computations $\overline{N}h = 0.6$ indicates that the estimate (6.13) is probably a more pessimistic one than it is actually required by computations, as it is often the case in numerical methods for ill-posed problems.

5. It seems to be at the first glance that because of (6.16), one can stop the iterative process at $n = 1$. However, our numerical experience shows that this way one cannot obtain good images. Here is a qualitative explanation of this. Equation (4.7) at $n = 1$ actually does not contain "a sufficient nonlinearity" if the parameter λ is sufficiently large (see (4.8)). It is known, on the other hand, that linearized inverse problems rarely image well high inclusions/background contrasts. The increase of n brings more nonlinearity in the process, because of terms with ∇q_i in (4.7). This nonlinearity, in turn enables one to image those contrasts well.

6. In terms of Remark 5.1 one can replace in Theorem 6.1 $\mathbb{R}^3$ with $\mathbb{R}^2$ and the proof will remain unchanged.

6.3 Proof of Theorem 6.1

This proof basically consists in estimating differences between our constructed functions $q_{n,k}, V_{n,k}$ and functions q_n^*, V_n^*. We are doing this using the Schauder theorem, (6.11) and (6.12). Since coefficients at lower order terms of our elliptic equations (5.4), (5.8) and (5.11) are changing with iterations, we need the condition (6.13) in order to have bounds for those coefficients for $n \leq \overline{N}$. First, we estimate the differences between functions $q_{1,k}$ and $q_1^*, k = 1, ..., m_1$. Denote

$$\widetilde{q}_{n,k} = q_{n,k} - q_n^*, \widetilde{V}_{n,k} = V_{n,k} - V^*, \widetilde{\psi}_n = \overline{\psi}_n - \overline{\psi}_n^*.$$

By (6.11) and (6.12)

$$\left\| \widetilde{V}_{1,1} \right\|_{C^{2+\alpha}(\overline{\Omega})} \leq 2\xi \leq M^*. \tag{6.15}$$

Substituting $n = 1$ in (6.8) and subtracting it from (5.1) and also subtracting (6.7) from (5.2), we obtain

$$\Delta \widetilde{q}_{1,1} - \varepsilon \widetilde{q}_{1,1} - A_{1,1} \nabla V_{1,1} \nabla \widetilde{q}_{1,1} = -2 \frac{I_{1,1}}{I_0} \left(\nabla q_1^* \right)^2 \tag{6.16}$$

$$-A_{1,1} \nabla \widetilde{V}_{1,1} \cdot \nabla q_1^* - A_{2,1} \nabla \widetilde{V}_{1,1} \left(\nabla V_{1,1} + \nabla V^* \right) - \varepsilon q^* - F_1,$$

$$\widetilde{q}_{1,1}(x) = \widetilde{\psi}_1(x), x \in \partial\Omega. \tag{6.17}$$

Hence, combining Schauder theorem with (4.8), (6.9), (6.10) and (6.15)-(6.17), we obtain

$$\| \widetilde{q}_{1,1} \|_{C^{2+\alpha}(\overline{\Omega})} \leq \frac{KM^*}{\lambda} \| \nabla q_1^* \|^2_{C^{\alpha}(\overline{\Omega})} + 3KM^* \eta. \tag{6.18}$$

First, let $k = 1$. Since $\| \nabla q_1^* \|_{C^{\alpha}(\overline{\Omega})} \leq M^*$, then (6.18) implies that

$$\| \widetilde{q}_{1,1} \|_{C^{2+\alpha}(\overline{\Omega})} \leq KM^* \left[\frac{(M^*)^2}{\lambda} + 3\eta \right].$$

Choose λ so large that

$$\frac{(M^*)^2}{\sqrt{\lambda}} \leq 1. \tag{6.19}$$

Hence,

$$\| \widetilde{q}_{1,1} \|_{C^{2+\alpha}(\overline{\Omega})} \leq KM^* \left(\frac{1}{\sqrt{\lambda}} + 3\eta \right), \tag{6.20}$$

$$\| q_{1,1} + q_1^* \|_{C^{2+\alpha}(\overline{\Omega})} \leq \| \widetilde{q}_{1,1} \|_{C^{2+\alpha}(\overline{\Omega})} + 2 \| q^* \|_{C^{2+\alpha}(\overline{\Omega})} \tag{6.21}$$

$$\leq KM^* \left(\frac{1}{\sqrt{\lambda}} + 3\eta \right) + 2M^* \leq 3M^*.$$

Using (3.10) and updating the tail as in Step 1^1 (section 5), we obtain from (6.20) and (6.21) that if $\eta_0 = \eta_0 \left(K(M^*, \Omega), M^*, \underline{s}, \overline{s}, d_1 \right) \in (0,1)$ is sufficiently small and $\eta \in (0, \eta_0)$, then the estimate (6.16) holds for the function $c_{1,1}$,

$$\| c_{1,1} - c^* \|_{C^{\alpha}(\overline{\Omega})} \leq 10K \left(M^* \right)^2 \left(1 + \overline{s}^2 \right) \left(\frac{1}{\sqrt{\lambda}} + 3\eta \right).$$

Since η is small and $c^* \geq 2d_1$, then $c_{1,1} \geq d_1$ in $\mathbb{R}^3$ (see Remark 5.2). Therefore by (6.11) and (5.3) $\left\| \widetilde{V}_{1,2} \right\|_{C^{2+\alpha}(\overline{\Omega})} \leq 2\xi$.

Estimate now $\|\widetilde{q}_{1,2}\|_{C^{2+\alpha}(\overline{\Omega})}$. Substituting $k=2$ in (5.4) and $n=1$ in (6.8), subtracting (6.8) from (5.4), as well as (6.7) from (5.2) and using (5.3), we obtain

$$\Delta\widetilde{q}_{1,2} - A_{1,1}\nabla V_{1,2}\nabla\widetilde{q}_{1,2} - \varepsilon\widetilde{q}_{1,2}$$

$$= -2\frac{I_{1,1}}{I_0}\left(\nabla\widetilde{q}_{1,1}\right)\left(\nabla q_{1,1} + \nabla q_1^*\right)$$

$$-A_{1,1}\nabla\widetilde{V}_{1,2}\nabla q_1^* - A_{2,1}\nabla\widetilde{V}_{1,2}\left(\nabla V_{1,2} + \nabla V^*\right) - \varepsilon q_1^* - F_1.$$

Hence, (6.20) and (6.21) imply that

$$\|\widetilde{q}_{1,2}\|_{C^{2+\alpha}(\overline{\Omega})} \leq \frac{3K\left(M^*\right)^2}{\lambda} KM^*\left(\frac{1}{\sqrt{\lambda}} + 3\eta\right) + 3KM^*\eta. \tag{6.22}$$

Choose μ such that in addition to (6.19)

$$\frac{6K\left(M^*\right)^2}{\lambda} < 1. \tag{6.23}$$

Then (6.22) leads to

$$\|\widetilde{q}_{1,2}\|_{C^{2+\alpha}(\overline{\Omega})} \leq 2KM^*\left(\frac{1}{\sqrt{\lambda}} + 3\eta\right), \tag{6.24}$$

and similarly with (6.21)

$$\|q_{1,2} + q_1^*\|_{C^{2+\alpha}(\overline{\Omega})} \leq 3M^*. \tag{6.25}$$

Hence, similarly with the above, (6.16) holds for the function $c_{1,2}$ and, therefore, $\left\|\widetilde{V}_{1,3}\right\|_{C^{2+\alpha}(\overline{\Omega})} \leq 2\xi$.

Consider now $\widetilde{q}_{1,3}$. Using (6.23) and (6.24), we obtain similarly with (6.22)

$$\|\widetilde{q}_{1,3}\|_{C^{2+\alpha}(\overline{\Omega})} \leq \frac{6K\left(M^*\right)^2}{\lambda} KM^*\left(\frac{1}{\sqrt{\lambda}} + 3\eta\right) + 3KM^*\eta \tag{6.26}$$

$$\leq 2KM^*\left(\frac{1}{\sqrt{\lambda}} + 3\eta\right).$$

Hence, similarly with (6.25)

$$\|q_{1,3} + q_1^*\|_{C^{2+\alpha}(\overline{\Omega})} \leq 3M^*. \tag{6.27}$$

Since the right hand sides of estimates (6.26) and (6.27) coincide with the right hand sides of estimates (6.24) and (6.25) respectively, then repeating this process m_1 times, we obtain using (5.5)

$$\|q_{1,m_1} - q_1^*\|_{C^{2+\alpha}(\overline{\Omega})} = \|q_1 - q_1^*\|_{C^{2+\alpha}(\overline{\Omega})} = \|\widetilde{q}_1\|_{C^{2+\alpha}(\overline{\Omega})} \leq 2KM^*\left(\frac{1}{\sqrt{\lambda}} + 3\eta\right),$$

$$\|q_{1,m_1}\|_{C^{2+\alpha}(\overline{\Omega})} = \|q_1\|_{C^{2+\alpha}(\overline{\Omega})} \leq 2M^*,$$

$$\|c_1 - c^*\|_{C^{\alpha}(\overline{\Omega})} \leq 10K\left(M^*\right)^2\left(1 + \overline{s}^2\right)\left(\frac{1}{\sqrt{\lambda}} + 3\eta\right).$$

Suppose that for $j = 1, ..., n-1$ and for $n < \overline{N}$ the estimates (6.14)-(6.16) hold, i.e.,

$$\left\|q_j - q_j^*\right\|_{C^{2+\alpha}(\overline{\Omega})} = \|\widetilde{q}_j\|_{C^{2+\alpha}(\overline{\Omega})} \leq 2KM^*\left(\frac{1}{\sqrt{\lambda}} + 3\eta\right), \tag{6.28}$$

$$\|q_j\|_{C^{2+\alpha}(\overline{\Omega})} \leq 2M^*, \tag{6.29}$$

$$\|c_j - c^*\|_{C^{\alpha}(\overline{\Omega})} \leq 10K\left(M^*\right)^2\left(1+\overline{s}^2\right)\left(\frac{1}{\sqrt{\lambda}}+3\eta\right). \tag{6.30}$$

We now prove that the same estimates are valid for $j := n$. Consider the function $q_{n,1}$. Subtracting (6.8) from (5.11) and (6.7) from (5.12), we obtain

$$\begin{aligned}
&\Delta\widetilde{q}_{n,1} - A_{1,n}\left(h\sum_{j=1}^{n-1}\nabla q_j(x)\right)\cdot\nabla\widetilde{q}_{n,1} + A_{1,n}\nabla V_{n,1}\cdot\nabla\widetilde{q}_{n,1} - \varepsilon\widetilde{q}_{n,1} \\
&= 2\frac{I_{1,n}}{I_0}\left[\nabla\widetilde{q}_{n,0}\left(\nabla q_{n0}+\nabla q_n^*\right)\right] \\
&+\left[A_{1,n}\nabla q_n^* - A_{2,n}h\sum_{j=1}^{n-1}\left(\nabla q_j+\nabla q_j^*\right)+2A_{2,n}\nabla V_{n,1}\right]\left(h\sum_{j=1}^{n-1}\nabla\widetilde{q}_j\right) \\
&+\left[2A_{2,n}h\sum_{j=1}^{n-1}\nabla q_j^* - A_{1,n}\nabla q_n^* - A_{2,n}\left(\nabla V_{n,1}+\nabla V^*\right)\right]\nabla\widetilde{V}_{n,1},
\end{aligned} \tag{6.31}$$

$$\widetilde{q}_{n,1}\mid_{\partial\Omega} = \widetilde{\psi}_n(x). \tag{6.32}$$

Estimate the second and third terms in the right hand side of (6.31). Using the definition of the number M^*, as well as (6.29), we obtain for the first part of the second term

$$\left|A_{1,n}\nabla q_n^* - A_{2,n}h\sum_{j=1}^{n-1}\left(\nabla q_j+\nabla q_j^*\right)+2A_{2,n}\nabla V_{n,1}\right| \leq M^*+3M^*\beta+M^* = 2M^*\left(1+\frac{3}{2}\beta\right).$$

On the other hand, by (6.28)

$$h\sum_{j=1}^{n-1}|\nabla\widetilde{q}_j| \leq 2KM^*\left(\frac{1}{\sqrt{\mu}}+3\eta\right)\overline{N}h = 2KM^*\left(\frac{1}{\sqrt{\lambda}}+3\eta\right)\beta.$$

Hence,

$$\begin{aligned}
&\left|A_{1,n}\nabla q_n^* - A_{2,n}h\sum_{j=1}^{n-1}\left(\nabla q_j+\nabla q_j^*\right)+2A_{2,n}\nabla V_{n,1}\right|\left|h\sum_{j=1}^{n-1}\nabla\widetilde{q}_j(x)\right| \\
&\leq 4K\left(M^*\right)^2\left(1+\frac{3}{2}M^*\beta\right)\left(\frac{1}{\sqrt{\lambda}}+3\eta\right)\beta.
\end{aligned} \tag{6.33}$$

Estimate now the third term in the right hand side of (6.31). Similarly with the above we obtain using (6.11)

$$\left|\left[2A_{2,n}h\sum_{j=1}^{n-1}\nabla q_j^* - A_{1,n}\nabla q_n^* - A_{2,n}\left(\nabla V_{n,1}+\nabla V^*\right)\right]\nabla\widetilde{V}_{n,1}\right| \leq M^*(1+\beta)\eta.$$

Combining this with (6.33), we obtain

$$\left|A_{1,n}\nabla q_n^* - A_{2,n}h\sum_{j=1}^{n-1}\left(\nabla q_j+\nabla q_j^*\right)+2A_{2,n}\nabla V_{n,1}\right|\left|h\sum_{j=1}^{n-1}\nabla\widetilde{q}_j(x)\right|$$

$$+\left|\left[2A_{2,n}h\sum_{j=1}^{n-1}\nabla q_j^*-A_{1,n}\nabla q_n^*-A_{2,n}\left(\nabla V_{n,1}+\nabla V^*\right)\right]\nabla\widetilde{V}_{n,1}\right| \tag{6.34}$$

$$\leq 4KM^*\left(1+\frac{3}{2}M^*\beta\right)\beta M^*\left(\frac{1}{\sqrt{\lambda}}+3\eta\right)+M^*\left(1+\beta\right)\eta.$$

Choose λ such that in addition to (6.19) and (6.23)

$$\frac{1}{\sqrt{\lambda}}\leq\eta. \tag{6.35}$$

Then using (6.13), we obtain

$$4KM^*\left(1+\frac{3}{2}M^*\beta\right)\beta M^*\left(\frac{1}{\sqrt{\lambda}}+3\eta\right)\leq 16KM^*\left(1+\frac{3}{2}M^*\beta\right)\beta M^*\eta\leq\frac{3}{2}M^*\eta.$$

Also, $M^*\left(1+\beta\right)\eta\leq 3/2M^*\eta$. Hence, we obtain from (6.34) and (6.35)

$$\left|A_{1,n}\nabla q_n^*-A_{2,n}h\sum_{j=1}^{n-1}\left(\nabla q_j+\nabla q_j^*\right)+2A_{2,n}\nabla V_{n,1}\right|\left|h\sum_{j=1}^{n-1}\nabla\widetilde{q}_j\left(x\right)\right|$$

$$+\left|\left[2A_{2,n}h\sum_{j=1}^{n-1}\nabla q_j^*-A_{1,n}\nabla q_n^*-A_{2,n}\left(\nabla V_{n,1}+\nabla V^*\right)\right]\nabla\widetilde{V}_{n,1}\right|\leq 3M^*\eta. \tag{6.36}$$

Recall that $V_{n,1}=V_{n-1,m_{n-1}}$. Hence, by (6.11), (6.13) and (6.28)-(6.30) coefficients at $\widetilde{q}_{n,1}$ in equation (6.31) do not exceed M^*. Hence, applying Schauder theorem to the Dirichlet boundary value problem (6.31), (6.32) and using (6.10) and (6.36), we obtain

$$\|\widetilde{q}_{n,1}\|_{C^{2+\alpha}\left(\overline{\Omega}\right)}\leq\frac{KM^*}{\lambda}\|\widetilde{q}_{n,0}\|_{C^{\alpha}\left(\overline{\Omega}\right)}\left(\|q_n\|_{C^{\alpha}\left(\overline{\Omega}\right)}+M^*\right)+3KM^*\eta. \tag{6.37}$$

Since by (5.7) $q_{n,0}=q_{n-1}$, then (6.28)-(6.30), (6.37) and (6.23) lead to

$$\|\widetilde{q}_{n,1}\|_{C^{2+\alpha}\left(\overline{\Omega}\right)}\leq\frac{6K\left(M^*\right)^2}{\lambda}KM^*\left(\frac{1}{\sqrt{\lambda}}+3\eta\right)+3KM^*\eta \tag{6.38}$$

$$\leq 2KM^*\left(\frac{1}{\sqrt{\lambda}}+3\eta\right).$$

Hence,

$$\|q_{n,1}+q_n^*\|_{C^{2+\alpha}\left(\overline{\Omega}\right)}\leq 3M^*. \tag{6.39}$$

Since the right hand sides of estimates (6.38) and (6.39) are the same as ones of estimates (6.26) and (6.27), from which estimates for functions q_1, $\widetilde{q}_1$ and c_1-c^* were derived, we obtain that estimates (6.28)-(6.30) are valid at $j=n$. This establishes estimates (6.14)-(6.16). To finish the proof, we note that only three conditions (6.19), (6.23) and (6.35) were imposed on the parameter λ. $\square$

7 Numerical Study

We test our algorithm for the problem in two dimensions.

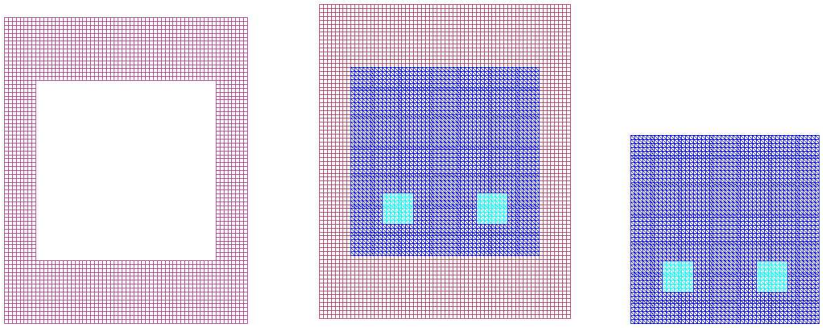

(a) G_{FDM} (b) $G = G_{FEM} \cup G_{FDM}$ (c) G_{FEM}

Figure 1: The hybrid mesh (b) is a combinations of a structured mesh (a), where FDM is applied, and a mesh (c), where we use FEM, with a thin overlapping of structured elements.

7.1 The Forward Problem

We now consider the above inverse problem for the time-dependent scalar wave equation modeling either acoustic or electric wave propagation (section 2) in a square $G \subset \mathbb{R}^2$ with the boundary $\partial G = \partial G_1 \cup \partial G_2 \cup \partial G_3$ (Figure 1). Here ∂G_1 and ∂G_2 are respectively top and bottom sides of the largest square of Figure 1 and ∂G_3 is the union of left and right sides of this square. The forward problem is

$$\begin{aligned} c(x)\frac{\partial^2 u}{\partial t^2} - \triangle u = 0, \quad & \text{in } G \times (0,T), \\ u(\cdot,0) = 0,\ \frac{\partial u}{\partial t}(\cdot,0) = 0, \ & \text{in } G, \\ \partial_n u\big|_{\partial G_1} = f(t), \ & \text{on } \partial G_1 \times (0,t_1], \\ \partial_n u\big|_{\partial G_1} = \partial_t u, \ & \text{on } \partial G_1 \times (t_1,T), \\ \partial_n u\big|_{\partial G_2} = \partial_t u, \ & \text{on } \partial G_2 \times (0,T), \\ \partial_n u\big|_{\partial G_3} = 0, \ & \text{on } \partial G_3 \times (0,T), \end{aligned} \tag{7.1}$$

where T is the final time. When calculating the Laplace transform (2.5) of the boundary data, we integrate for $t \in (0,T)$, thus calculating an approximation of this transform. The plane wave f is initialized at the top boundary ∂G_1 of the computational domain G, propagates during the time period $(0,t_1]$ into G, is absorbed at the bottom boundary ∂G_2 for all times $t \in (0,T)$ and it is also absorbed at the top boundary ∂G_1 for times $t \in (t_1,T)$. Here

$$f(t)\big|_{\Gamma_1} = \frac{(\sin(\overline{s}t - \pi/2) + 1)}{10}, \ 0 \le t \le \frac{2\pi}{\overline{s}}, \tag{7.2}$$

We are interested in the reconstruction of the coefficient $c(x)$, which is the wave speed $1/\sqrt{c(x)}$ in the case of acoustics and the product $(\mu\epsilon)(x) = c(x)$ of magnetic permeability and electric permittivity in the EM case. The asymptotic behavior (2.12) will be verified computationally.

The computational domain in all our tests $G = G_{FEM} \cup G_{FDM}$ is set as $G = [-4.0, 4.0] \times [-5.0, 5.0]$. This domain is split into a finite element domain $G_{FEM} = [-3.0, 3.0] \times [-3.0, 3.0]$ and a surrounding domain G_{FDM}, see Figure 1. The space mesh in Ω_{FEM} consists of triangles and in Ω_{FDM} of squares, with mesh size in the overlapping regions $\tilde{h} = 0.125$. We apply the hybrid finite element/difference method presented in [5] where

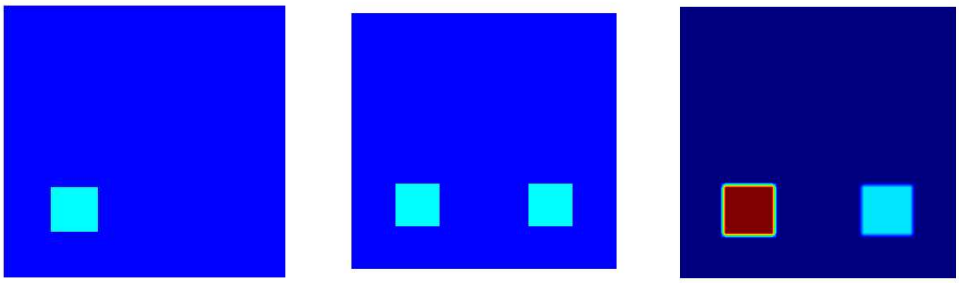

(a) G_{FEM_1} (b) G_{FEM_2} (c) G_{FEM_3}

Figure 2: Computational domains

finite elements are used in G_{FEM} and finite differences in G_{FDM}. At the top and bottom boundaries of G we use first-order absorbing boundary conditions [12] which are exact in this particular case. At the lateral boundaries, mirror boundary conditions allow us to assume an infinite space domain in the lateral direction.

In real applications the data are generated by emitting waves on the surface of the investigated object and are then recorded on parts of the surface of the object. In this paper, we work with the computationally simulated data. That is, the data are generated by computing the forward problem (7.1) with the given function $c(x)$. The corresponding solution is recorded at the entire boundary then. Next, the coefficient $c(x)$ is "forgotten", and the goal is to reconstruct this coefficient from the Dirichlet boundary data given at the boundary of the subdomain $G_{FEM} \subset G$, which are computed along with the solution of the forward problem. We assume that $c = 1$ in Ω_{FDM}. Thus, we need to reconstruct the coefficient $c(x)$ only in G_{FEM}.

7.2 A hybrid finite element/difference method for the forward problem (7.1)

To solve the forward problem (7.1), we use the hybrid FEM/FDM method described in [4] and [5]. This method uses continuous space-time piecewise linear finite elements on a partially structured mesh in space. The computational domain G is decomposed into a finite element domain Ω_{FEM} (the same as G_{FEM} above) with an unstructured mesh and a finite difference domain Ω_{FDM} (the same as G_{FEM} above) with a structured mesh, see Figure 1. In Ω_{FDM} we use quadrilateral elements in $\mathbb{R}^2$ and hexahedra in $\mathbb{R}^3$. In Ω_{FEM} we use a finite element mesh $K_h = \{K\}$ with elements K consisting of triangles in $\mathbb{R}^2$ and tetrahedra in $\mathbb{R}^3$. We associate with K_h a mesh function $\widetilde{h} = \widetilde{h}(x)$ representing the diameter of the element K containing x. For the time discretization we let $J_k = \{J\}$ be a partition of the time interval $I = (0, T)$ into time intervals $J = (t_{k-1}, t_k]$ of uniform length $\tau = t_k - t_{k-1}$.

7.3 Results of reconstruction

In this subsection we present results of our reconstructions. We have used solution of the forward problem (7.1) in the domain G to generate the data at the boundary of the square $\Omega := \Omega_{FEM}$. We have performed numerical experiments to reconstruct the medium, which is homogeneous with $c(x) = 1$ except of either two small squares or a single square, see Figure 2. But we have not assumed *a priori* knowledge of neither the structure of this medium nor of the background constant $c(x) = 1$ outside of those squares. To produce updates for tails, we have solved on each iterative step the forward problem (7.1) instead

of solving the problem (2.9), (2.10). Next, we have calculated the Laplace transform (2.5) of the solution to obtain the function $w(x,\overline{s})$.

In all our numerical experiments we have chosen the step size with respect to the pseudo frequency $h = 0.05$, the s-interval $[\underline{s},\overline{s}]$=$[6.7, 7.45]$. Hence, $N = 15$ in our case. We have chosen two sequences of regularization parameters $\lambda := \lambda_n$ and $\varepsilon = \varepsilon_n$ for $n = 1, ..., N$. Both the formulation and the proof of Theorem 6.1 remain almost unchanged for this case. The reason of choosing different values of λ_n and ε_n is that values of functions q_1 and q_2 and their gradients are very small. Hence, in order not to eliminate totally the influence of the nonlinear term $(\nabla q_{n,k-1})^2, n = 1, 2$ in (5.4), (5.8) and (5.11), the values of λ_1 and λ_2 should not be too large. Next, the values of nonlinear terms start to grow, and we balance them via taking a larger value of λ_n for $n = 3, 4, 5$. For $n > 5$ the values of nonlinear terms become even bigger, and we balance them via taking increasing again the value of λ_n. This once again points towards the importance of the introduction of CWFs in the numerical scheme, as compared with the decrease of the step size h. The considerations for choosing different values of ε_n are similar. In *all* Tests 1-4 the values of the parameters λ_n and ε_n were:

$$\begin{aligned} &\lambda_n = 20, n = 1, 2; \lambda_n = 200, n = 3, 4, 5; \lambda_n = 2000, n \geq 6; \\ &\varepsilon_n = 0, n = 1, 2; \varepsilon_n = 0.001, n = 3, 4, 5; \varepsilon_n = 0.01, n = 6, 7, \\ &\varepsilon_n = 0.1, n \geq 8. \end{aligned} \tag{7.3}$$

Once the function $q_{n,k}$ is calculated, we update the function $c := c_{n,k}$ using formulas (3.7), (3.10). To find second derivatives in (3.10), we use the standard finite difference approximations of both the Laplacian and the gradient on a structured Cartesian mesh. More precisely, in two dimensions we use following approximation to find $c(x)$ at point (i, j):

$$\begin{aligned} c_{i,j} = &\frac{\tilde{v}_{i+1,j} - 2\tilde{v}_{i,j} + \tilde{v}_{i-1,j}}{dx^2} + \frac{\tilde{v}_{i,j+1} - 2\tilde{v}_{i,j} + \tilde{v}_{i,j-1}}{dy^2} \\ &+ \underline{s}^2 \left(\left(\frac{\tilde{v}_{i+1,j} - \tilde{v}_{i,j}}{dx} \right)^2 + \left(\frac{\tilde{v}_{i,j+1} - \tilde{v}_{i,j}}{dy} \right)^2 \right), \end{aligned} \tag{7.4}$$

where dx and dy are grid step sizes of the discrete finite difference mesh in the directions x and y respectively. We enforce that the parameter $c(x)$ belongs to the set of the admissible parameters $C_M = \{c \in C(\overline{\Omega}) \mid 0.5 \leq c(x) \leq 7\}$ as follows: if $c_{n,k}(x_0) < 0.5$ for a certain point $x_0 \in \Omega$ and a certain pair (n, k), then we set $c_{n,k}(x_0) := 1$ by putting the box constrains on the computed parameters. We also use the smoothness indicator in update values of $c(x)$ by local averaging over the neighboring elements.

Thus, the resulting computed function is $c(x) := c_{\overline{N}}(x)$. Recall that the number of iterations is the vectorial regularization parameter in our case (see Remarks 6.2). One of the backbones of the theory of ill-posed problems is that regularization parameters depend on the range of parameters for a specific problem one considers. Thus, our choice of regularization parameters is in an agreement with this concept. For the above values of $h, \underline{s}, \overline{s}$ and the range of the target coefficient $c(x) \in [1, 4]$ we have used $m_n = 4$ iterations with respect to tails for $n \leq n_0$ and $m_n = 7$ for $n = n_0 + 1, ..., \overline{N}$, where numbers n_0 and $\overline{N}$ are chosen on the basis of an *objective* stopping rule described below. Hence, while the pairs $(n_0, \overline{N})$ differ in our tests, the rule of their choice (i.e., the stopping rule) remains the same. As it is always the case in ill-posed problems, the choice of proper regularization parameters and of a proper stopping rule was time consuming. However, we point out that

our stopping rule, as well as regularization parameters $\lambda_n, \varepsilon_n, m_n$, once chosen, remained *the same for all* our numerical experiments described in Tests 1-4 below. Hence, results were not "conveniently adjusted" for each specific test in order to obtain the best possible image for that test.

The Dirichlet boundary value problems in the square Ω_{FEM} for functions $q_{n,k}$ were solved by the FEM, in which the same finite elements were used as ones in the forward problem (7.1) in the domain Ω_{FEM}. The "inverse crime" was avoided because the forward problem was solved for the hyperbolic equation, whereas we solve an elliptic equation on each step of the reconstruction algorithm. In addition, we have added a random noise to the boundary data. The FEM cannot guarantee that resulting functions $q_{n,k} \in C^{2+\alpha}\left(\overline{\Omega}\right)$, as it is required by Theorem 6.1. And also the above "adjustment" of computed values $c_{n,k}(x_0)$ by box constraint does not guarantee that the resulting function $c_{n,k} \in C^{\alpha}\left(\overline{\Omega}\right)$. Such discrepancies quite often take place in computations and are, therefore acceptable in numerical studies. Nevertheless, an analogue of Theorem 6.1 can be proved for the discrete case when the FEM analogues of equations for functions $q_{n,k}$ are used, and also the domain Ω with $\partial\Omega \in C^3$ is replaced respectively with either a rectangular prism in $\mathbb{R}^3$ or a rectangle in $\mathbb{R}^2$, as in our numerical examples. To prove this analogue, one needs to use the weak formulations of these equations and the Lax-Milgram theorem instead of the Schauder theorem. Next, because of the equivalency of norms in finite dimensional spaces, the rest of the proof of Theorem 6.1 remains almost the same. However, the latter development is outside of the scope of this publication and might be considered in our future works. Another interesting question here is about the change of reconstructed images due to the increase of the number of finite elements, because that equivalency of norms "worsens" with the increase of the dimension of the space. This question might also be addressed in future publications.

In all our tests we compute multiplicative random noise in the boundary data, u_σ, by adding relative error to computed data u_{obs} using expression

$$u_\sigma\left(x^i, t^j\right) = u_{obs}\left(x^i, t^j\right)\left[1 + \frac{\alpha_j(u_{max} - u_{min})\sigma}{100}\right]. \tag{7.4}$$

Here, $u_{obs}\left(x^i, t^j\right) = u\left(x^i, t^j\right), x^i \in \partial\Omega_{\text{FEM}}$ is a mesh point at the boundary $\partial\Omega_{\text{FEM}}, t^j \in (0, T)$ is the mesh point in time, α_j is a random number in the interval $[-1; 1]$, u_{max} and u_{min} are maximal and minimal values of the computed data u_{obs}, respectively, and σ is the noise level in percents. Next, we make the Laplace transform (2.5) of the data, which helps to both "smooth out" and decrease the noise, due to the integration. Because of that, we have successfully used the following formula for the $s-$derivative of the boundary data $\varphi(x, s)$ in (2.13) to obtain the function $\psi(x, s_n)$ in (3.9)

$$\psi(x, s_n) \approx \frac{\varphi(x, s_{n-1}) - \varphi(x, s_n)}{h}, h = 0.05.$$

In all our tests 1-4 we have verified numerically the asymptotic behavior (3.4). To do this, we have considered functions $g_1(s)$ and $g_2(s)$, for $s \in [6.5, 7.5] \supset [\underline{s}, \overline{s}] = [6.7, 7.45]$, where

$$g_1(s) = s\left\|\nabla\widetilde{v}(x, s)\right\|_{L_2(\Omega_{FEM})}, g_2(s) = s\left\|\nabla q(x, s)\right\|_{L_2(\Omega_{FEM})},$$

where functions $\widetilde{v}(x, s)$ and $q(x, s)$ are taken from the solution of the forward problem. Their graphs (not shown) have shown that these functions are very close to constants for $s \in [6.5, 7.5]$, which corresponds well with (3.4). We have also verified numerically in all our examples 1-4 that the function $w(x, s) > 0$, which justifies the introduction of the function $\widetilde{v}(x, s) = \ln w(x, s)/s^2$.

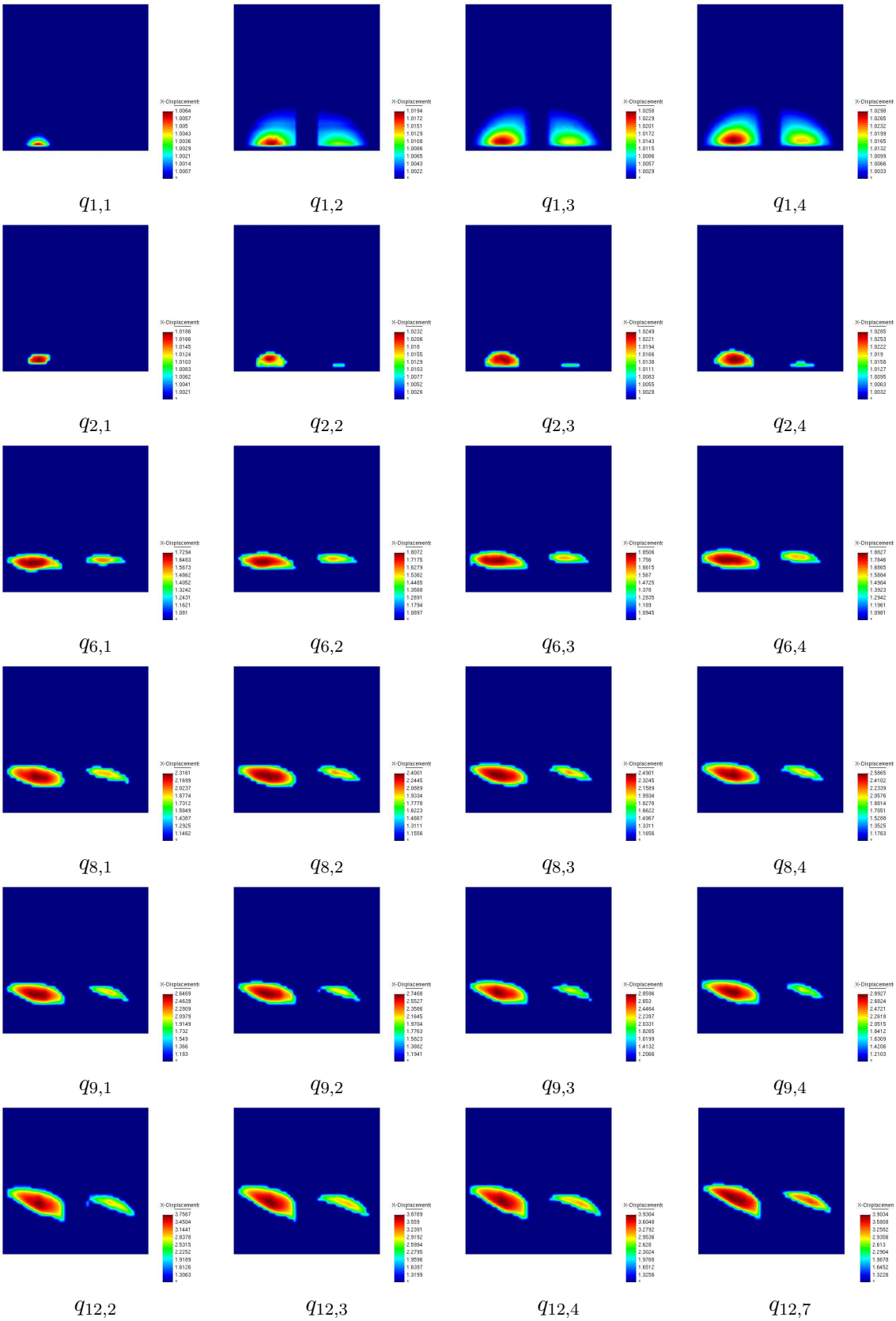

Figure 3: Test 1: spatial distribution of c_h after computing $q_{n,i}; n = 1, 2, 6, 8, 9, 12,$, where n is number of the computed function q.

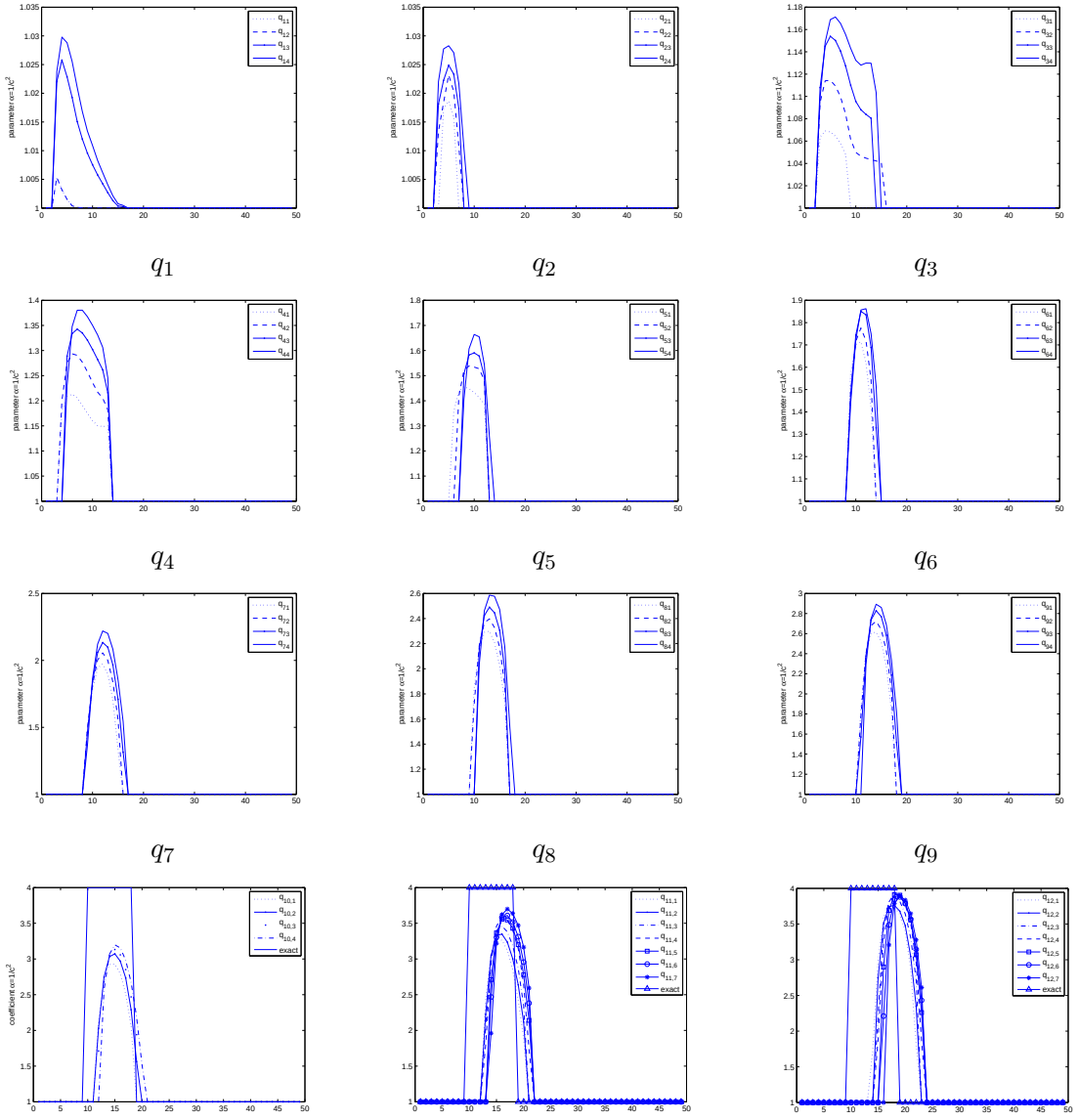

q_1 q_2 q_3

q_4 q_5 q_6

q_7 q_8 q_9

q_{10} q_{11} q_{12}

Figure 4: Test 1: the one-dimensional cross-sections of the image of the function c_{comp} along the vertical line connecting the points $(-1.5, -3)$ and $(-1.5, 3)$ computed for corresponding functions $q_n, n = 1, ..., 12$.

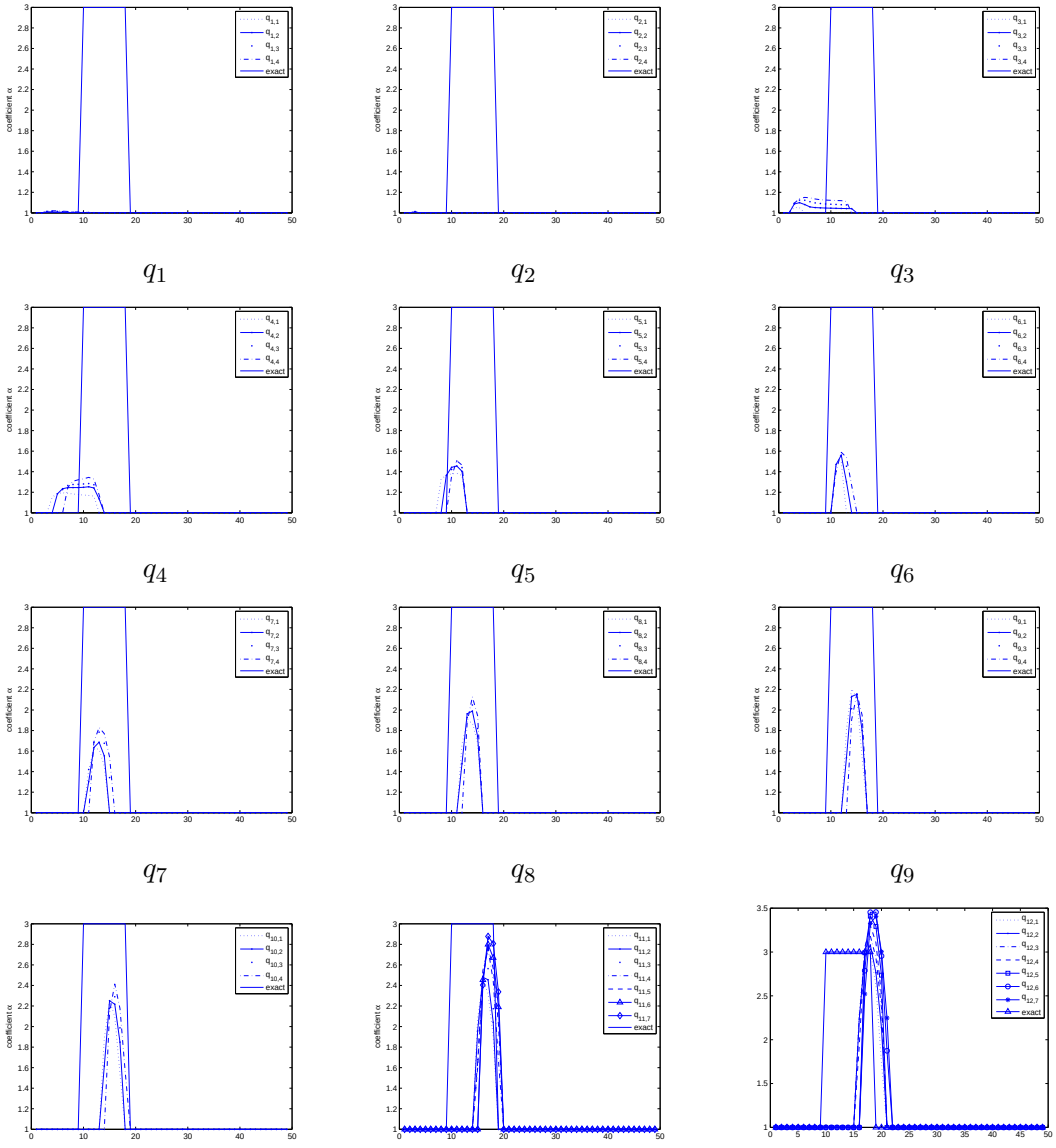

q_1 q_2 q_3

q_4 q_5 q_6

q_7 q_8 q_9

q_{10} q_{11} q_{12}

Figure 5: Test 1: the one-dimensional cross-sections of the image of the function c_{comp} along the vertical line connecting the points $(-2.5, -3)$ and $(-2.5, 3)$ computed for corresponding functions $q_n, n = 1, ..., 12$.

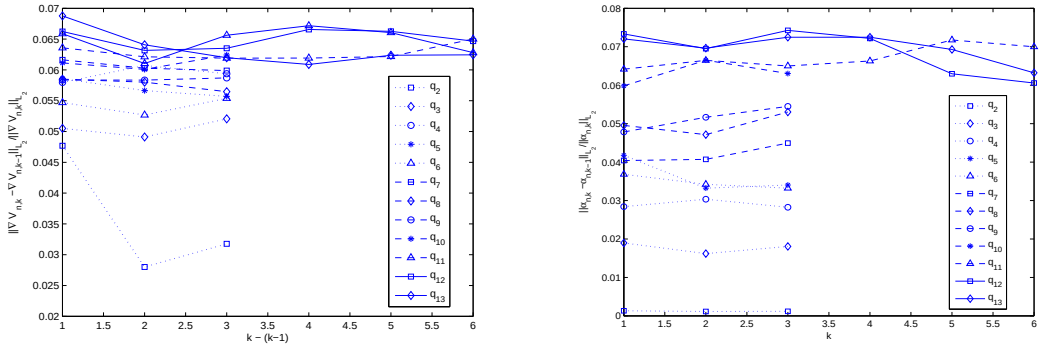

a) b)

.

Figure 6: Test 1: Computed relative L_2-norms: a) of the $\frac{||\nabla V_{n,k}-\nabla V_{n,k-1}||}{||\nabla V_{n,k}||}$; b) of the $\frac{||c_{n,k}-c_{n,k-1}||}{||c_{n,k}||}$

Test 1. We test our numerical method on the reconstruction of the structure given on Figure 2-c). We take $c = 4$ in the left small square of Figure 2-c), $c = 3$ in the right square and $c = 1$ everywhere else. We take the starting value for the tail $V_{1,1}(x, \overline{s}) \equiv 0$. We introduce $\sigma = 10\%$ of the multiplicative random noise in the boundary data u_{obs} by the formula (7.4).

Figure 3 displays isosurfaces of resulting images for $q_{n,k}, n = 1, 2, 6, 8, 9, 12; k = 1, ..., 4$. Figure 4 presents the one-dimensional cross-sections of the image of the computed functions $c_{n,k}$ along the vertical line passing through the middle of the left small square. Comparison of images of functions $c_{n,k}$ for different values n and k shows that the inclusion/background contrasts grow with the grow of n and k. In particular, these contrasts are very low for $n = k = 1$ and do not exceed $1.006/1$. On the last three images of Figure 4 the computed functions $c_{n,k}$ for $n = 10, 11, 12$ are superimposed with the correct one.

Figure 5 displays the one-dimensional cross-sections of the image of the functions $c_{n,k}$ along the vertical line passing through the middle of the right small square superimposed with the correct one. One can see that the $4 : 1$ contrast in the left square is imaged accurately. As to the right square, we got the $3.5 : 1$ contrast. The function $c(x) = 1$ outside of these squares is also imaged accurately. Locations of imaged inclusions are somewhat shifted upwards.

We now explain our *stopping criterion*. Figure 6-a) shows computed relative L_2-norms of gradients of tails

$$\frac{||\nabla V_{n,k} - \nabla V_{n,k-1}||}{||\nabla V_{n,k}||} \tag{7.5}$$

and Figure 6-b) - shows relative L_2-norms of the target coefficient

$$\frac{||c_{n,k} - c_{n,k-1}||}{||c_{n,k}||}. \tag{7.6}$$

We use these norms as the stopping rule for computation in our iterative algorithm. We stop our iterative algorithm for computing of the new function q_n when both relative norms (7.5) and (7.6) are stabilized. Here is how we do this. First, we observe on Figure 6-a) that relative L_2-norms (7.5) of the computed gradients of tails grow until $n = 10$. For $n \geq 10$ norms (7.5) change slowly. Thus, we conclude that at q_9 tails are stabilized. However, norms (7.6) still grow for $n > n_0 = 9$, see Figure 6-b). We repeat our iterative procedure

for $n = 10, 11, 12, 13$. And for $n \geq 10$ we also increase the number of iterations with respect to tails: we now take 7 iterations instead of 4. We observe that at $n = 12$ both relative norms (7.5) and (7.6) are stabilized. Thus, we set $\overline{N} = 12$ and we take $c_{12,7}(x)$ as our final reconstructed image. On the Figure 6 we also present results for $n = 13$, as a confirmation that norms (7.5) and (7.6) are stabilized.

Remark 7.1. At the same time, we have observed that for $n = 14, 15$ norms (7.6) abruptly grow, which was reflected in an abrupt move of positions of imaged inclusions upwards (not shown). This confirms that our choice of $\overline{N}$, which is one of regularization parameters here (see item 4 in Remarks 6.2) was correct one. A similar behavior was observed in Tests 2 and 3. We use exactly the same stopping criterion in Tests 2,3,4. However, the number $\overline{N}$ is different for each of these examples, so as the number n_0 at which relative norms (7.5) of gradients tails are stabilized. The fact that these two numbers change from one example to another one points towards robustness of our stopping rule.

Test 2. We now test our numerical method on the reconstruction of the structure given on Figure 2-b). We take the starting value for the tail $V_{1,1}(x, \overline{s}) \equiv 0$. We compute $\sigma = 5\%$ of the multiplicative random noise in the boundary data u_{obs} by the formula (7.4). We take $c = 4$ for both small squares of Figure 2-b) and $c = 1$ outside of these squares. Hence, the inclusion/background contrast is $4 : 1$, which is quite high in inverse problems. Figures 7 - 8 present isosurfaces of resulting images of the functions $c_{n,k}$ after computing functions $q_{n,k}, n = 1, 2, ..., 12$. Figure 9 presents the one-dimensional cross-section of the image of the function $c_{n,k}$ along the vertical line passing through the middle of the left small square. The imaged function $c(x)$ is superimposed with the correct one. One can see that the value of the function $c(x)$ both inside and outside of the inclusion is imaged correctly (including the $4 : 1$ contrast), although the location of the inclusion is somewhat shifted to the top.

We have used the same stopping rule as above and thus discovered that $n_0 = 9$ and $\overline{N} = 12$. The behavior of norms (7.5) and (7.6) (not shown) was similar with one on Figure 6. The last image on Figure 8 represents the final $c_{12,7}$ image of the target coefficient $c(x)$.

Test 3. We now consider only a single small square of Figure 2-a), the left one, with $c = 3$ in it, leaving all other parameters the same as above. Again we take the starting value for the tail $V_{1,1}(x, \overline{s}) \equiv 0$. Now we perform computations with $\sigma = 5, 15\%$ of the multiplicative random noise in the boundary data u_{obs}.

Figure 10 displays isosurfaces of images for $q_{n,k}, n = 2, 5, 7, 8, 10$ with 5% noise in the boundary data. Figure 11 displays isosurfaces of images for $q_{10,k}$ with 15% noise in the boundary data. Figure 12 presents one-dimensional cross-sections of the image of functions $c_{n,k}$ computed with q_9, q_{10} and q_{11} along the vertical line passing through the center of this square. The imaged function $c(x)$ is superimposed with the correct one. We observe that we obtain the $3.2 : 1$ contrast of the reconstructed function $c(x) := c_{10,7}(x)$, which is quite accurate, since the correct contrast is $3 : 1$.

Figure 13 shows computed relative L_2-norms (7.5) and (7.6) with noise level $\sigma = 5\%$ in data. As in previous examples, we use these norms as the stopping rule in our iterative algorithm. Using Figure 13, we analyze results of the reconstruction. On Figure 13-a) we observe that relative L_2-norms (7.5) of the computed gradients of tails grow until computing the function q_7. After that tails change slowly, which means that $n_0 = 7$. However, norms (7.6) are not yet stabilized. Hence, we now want to stabilize norms (7.6). We repeat our iterative procedure for $n = 8, 9, 10, 11$ and with 7 iterations with respect to tails for these values of n instead of previous 4. On Figure 13-b) we observe that at q_9 both norms (7.5) and (7.6) are stabilized, and at q_{10}, q_{11} these norms almost do not change, although the norm for $q_{11,7}$ starts to grow. Thus, we conclude, that we achieve solution of our problem at $q_{10} = q_{10,7}$ with $\overline{N} = 10$. We have observed a similar behavior of our solution with

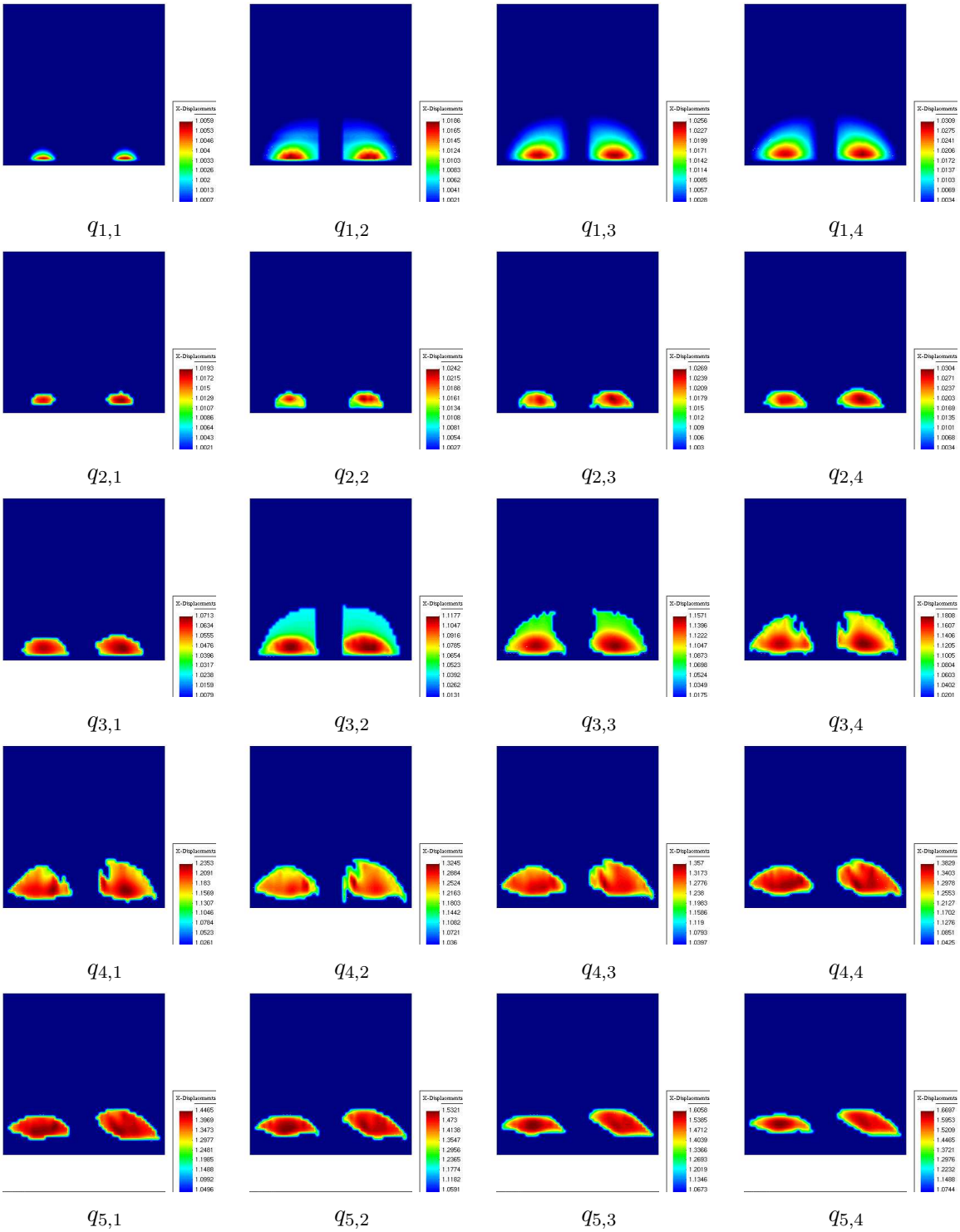

Figure 7: Test 2: spatial distribution of c_h after computing $q_{n,i}; n = 1, ...5,$, where n is number of the computed function q.

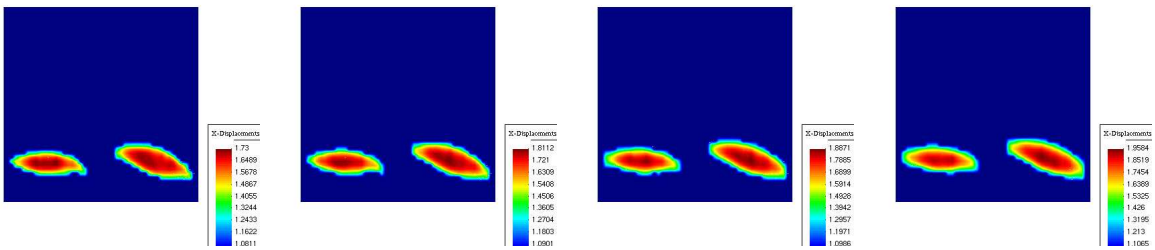

$q_{6,1}$ $q_{6,2}$ $q_{6,3}$ $q_{6,4}$

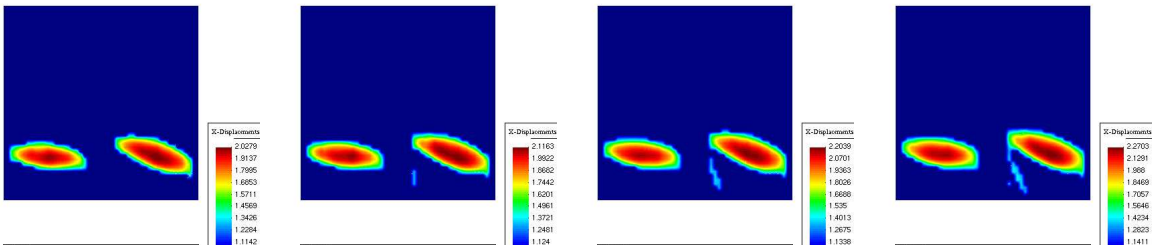

$q_{7,1}$ $q_{7,2}$ $q_{7,3}$ $q_{7,4}$

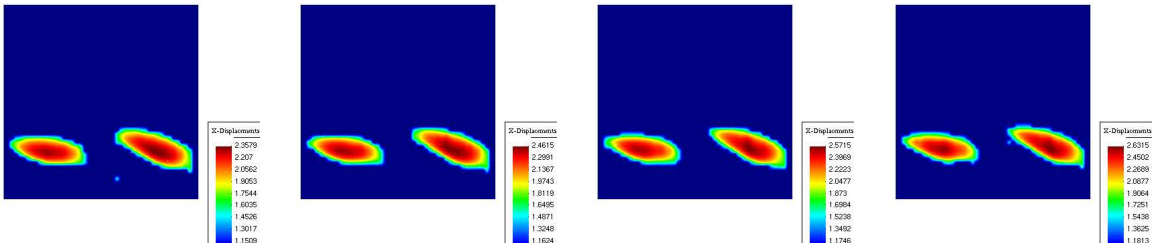

$q_{8,1}$ $q_{8,2}$ $q_{8,3}$ $q_{8,4}$

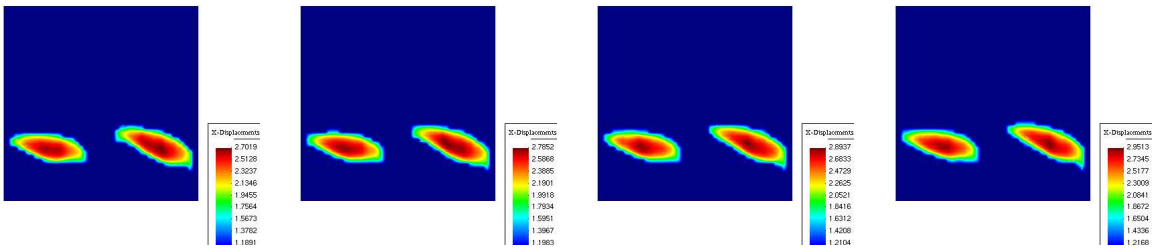

$q_{9,1}$ $q_{9,2}$ $q_{9,3}$ $q_{9,4}$

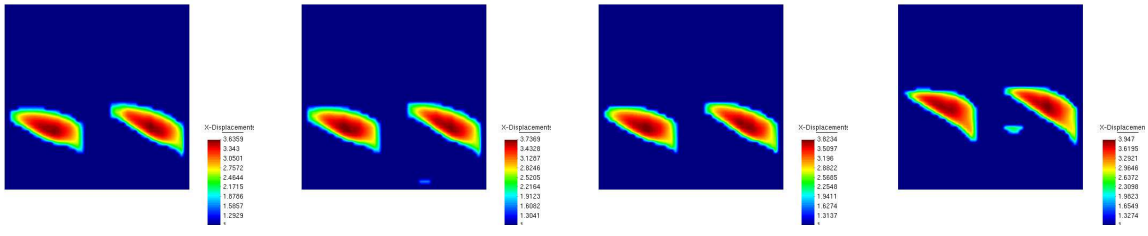

$q_{12,1}$ $q_{12,2}$ $q_{12,3}$ $q_{12,7}$

Figure 8: Test 2: spatial distribution of c_h after computing $q_{n,i}; n = 6, 7, 8, 9, 12,$ where n is number of the computed function q.

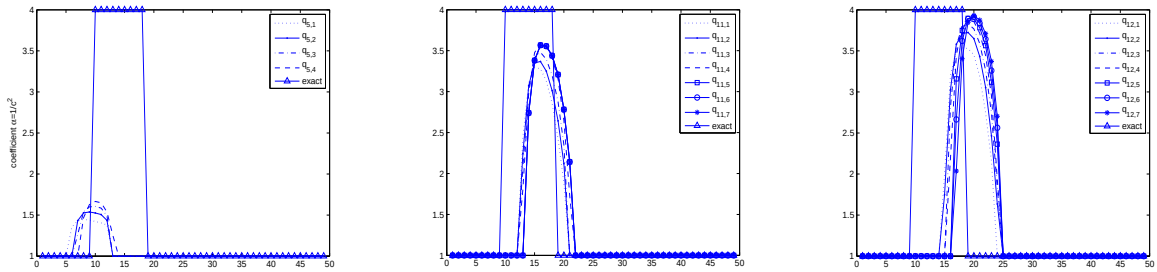

q_5 q_{11} q_{12}

Figure 9: Test 2: the one-dimensional cross-sections of the image of the function c_{comp} along the vertical line connecting the points $(-1.5,-3)$ and $(-1.5,3)$.

the relative noise level $\sigma = 15\%$. Similarly with Tests 1 and 2 we have observed that norms (7.5) and (7.6) abruptly increase at q_{12}. Thus we can conclude that our choice of the iteration number $\overline{N} = 10$ as a regularization parameter is correct one.

Test 4. The goal of this experiment is to confirm that the error in the reconstructed images is mainly determined by the truncation error, as it follows from Theorem 6.1, see the second remark after Theorem 6.1. We now consider the same parameters, as ones in previous tests, except that we take the exact initial tail $V_{1,1}(x,\overline{s}) = V^*(x,\overline{s})$ and the noise level $\sigma = 5\%$. We use the same iterative algorithm and the same regularization parameters as in all previous tests. We stop our iterative algorithm for computation of the new function q_n after computing the function q_1, since relative L_2-norms $\frac{||c_{1,k}-c_{1,k-1}||}{||c_{1,k}||} = 0$ and $\frac{||\nabla V_{1,k}-\nabla V_{1,k-1}||}{||\nabla V_{1,k}||} = 0$ for all $k > 1$.

On Figure 14-a) $c = 4$ in the left small square and $c = 3$ in the right small square (as in Test 1). On Figure 14-b) $c = 4$ in both small squares (as in Test 2), and $c = 3$ in the one small square on Figure 14-c) (as in Test 3). One can observe that the reconstruction is almost an ideal one, and even shapes of inclusions resemble well the correct ones. It is not fully ideal because of inevitable computational errors, the approximation of the function $q(x,s)$ by a piecewise constant function with respect to s and the 5% noise in the data. The latter goes along well with Theorem 6.1: see the parameter η in it.

Test 5. We now show that without a globally convergent algorithm the same images deteriorate, if the good first guess for the solution is unknown. To do this, we use the locally convergent reconstruction algorithm described in [4], where the inverse problem is formulated as an optimal control problem. We find a stationary point of a Lagrangian, using the forward wave equation (the state equation), the backward wave equation (the adjoint equation), and an equation, which reflects the fact that the gradient with respect to the parameters should vanish. A minimizer of a corresponding least squares objective functional is found via an iterative procedure via solving for the forward and backward wave equations for each iterative step and updating the material coefficients. We generate the data for the inverse problem using the same computational mesh and the same parameters as ones in Test 2. We start the optimization algorithm with different values of the first guess for the parameter $c_{guess} = const.$ at all points of the computational domain Ω_{FEM}. Figure 15 presents the images of the computed function c_{comp}. for the following initial guesses: on a) $c_{guess} = 1.0$, on b) $c_{guess} = 1.5$, and on c) $c_{guess} = 2.0$. We observe that images deteriorate if the good first guess for the solution is unknown. Most likely, local minima are achieved in all these three cases.

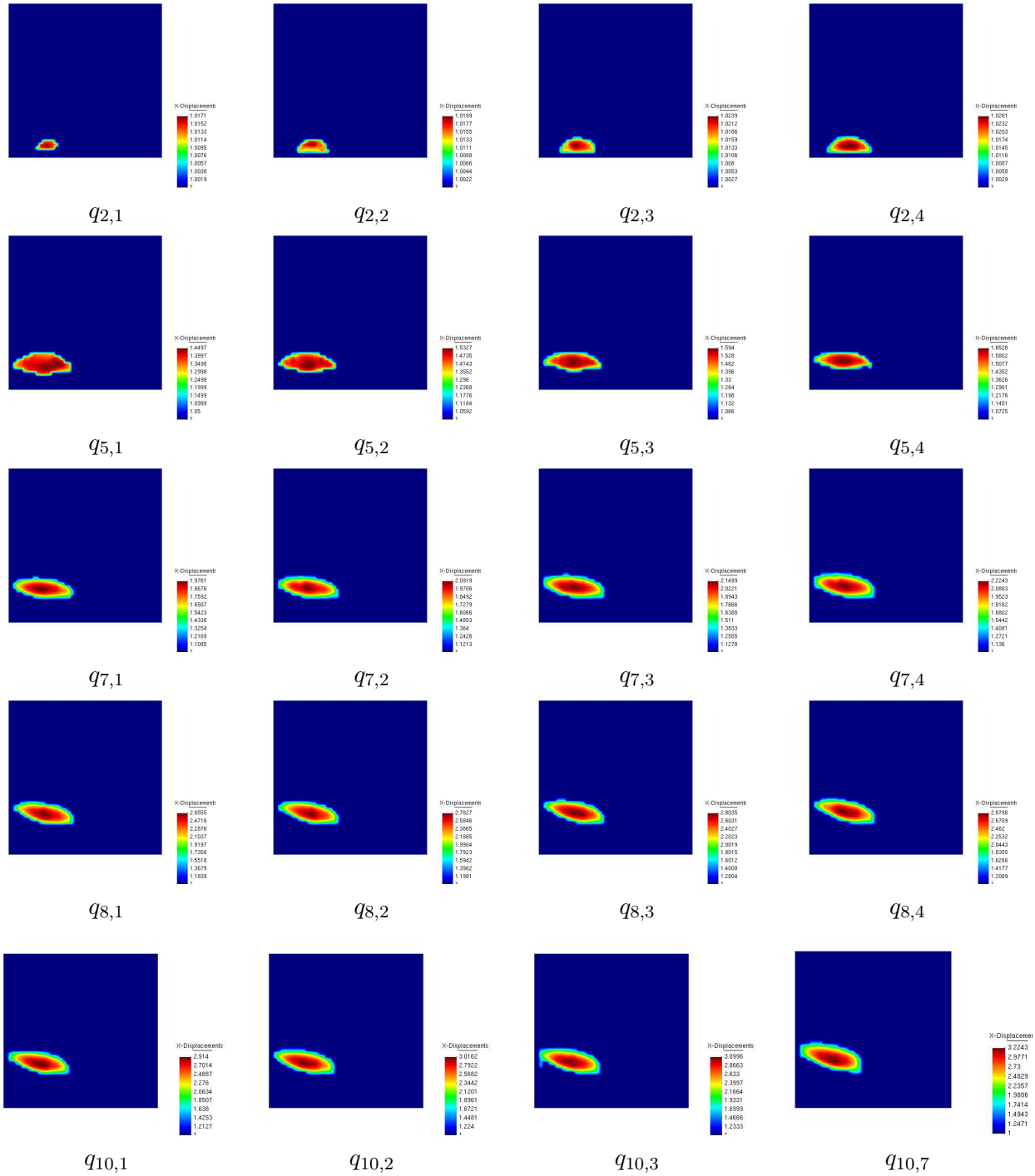

Figure 10: Test 3: Reconstruction with 5 % relative noise in data. We present spatial distribution of c_h after computing $q_{n,i}; n = 2, 5, 7, 8, 10$, where n is number of the computed function q.

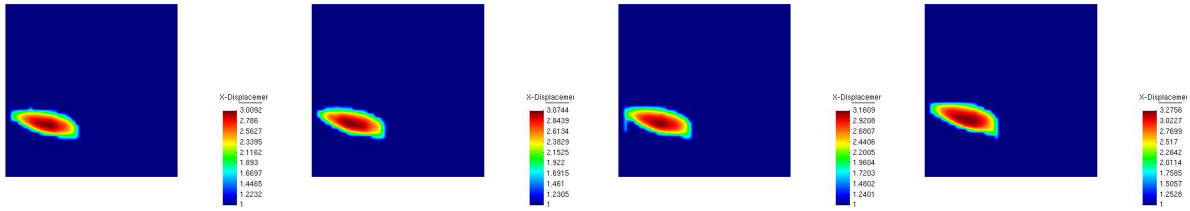

$q_{10,1}$ $q_{10,2}$ $q_{10,3}$ $q_{10,7}$

Figure 11: Test 3: Reconstruction with 15 % relative noise in data. We present spatial distribution of c_h after computing $q_{12,i}$.

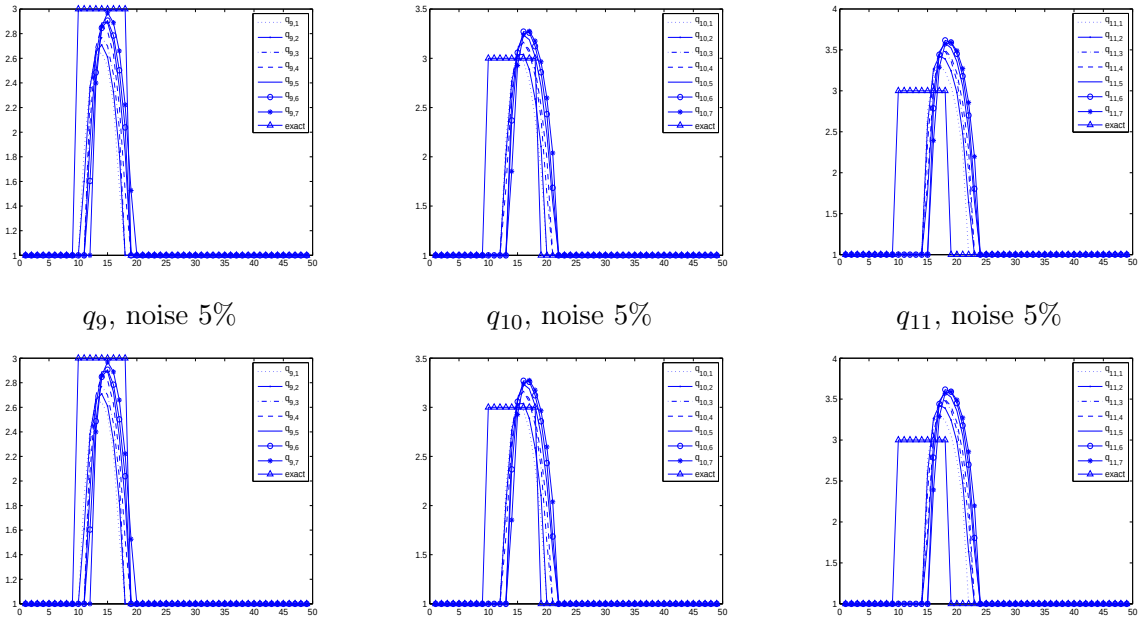

q_9, noise 5% q_{10}, noise 5% q_{11}, noise 5%

q_9, noise 15% q_{10}, noise 15% q_{11}, noise 15%

Figure 12: Test 3: the one-dimensional cross-sections of the image of the function c_{comp} along the vertical line connecting the points $(-1.5, -3)$ and $(-1.5, 3)$.

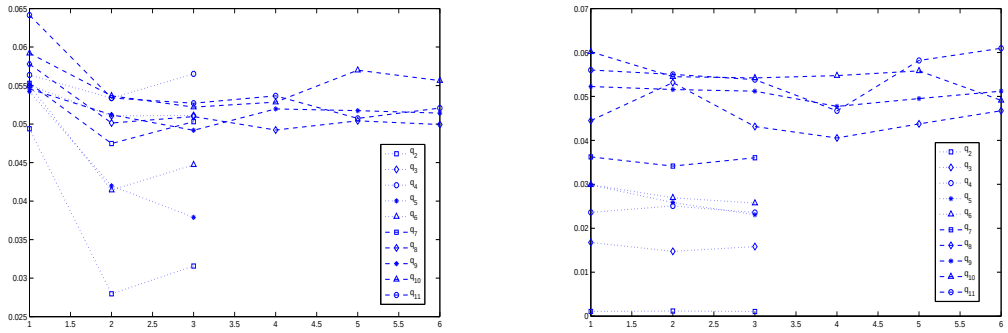

a) $\sigma = 5\%$ b) $\sigma = 5\%$

Figure 13: Test 3: Computed relative L_2-norms: a) $\frac{||\nabla V_{n,k} - \nabla V_{n,k-1}||}{||\nabla V_{n,k}||}$; b) $\frac{||c_{n,k} - c_{n,k-1}||}{||c_{n,k}||}$

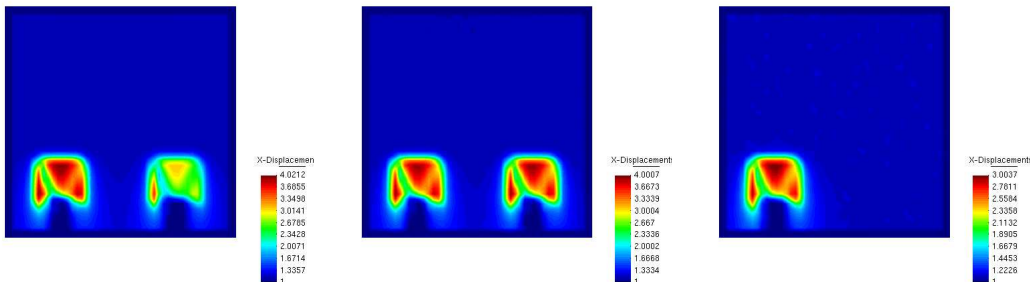

a) b) c)

Figure 14: Test 4: spatial distribution of c_h with exact tail.

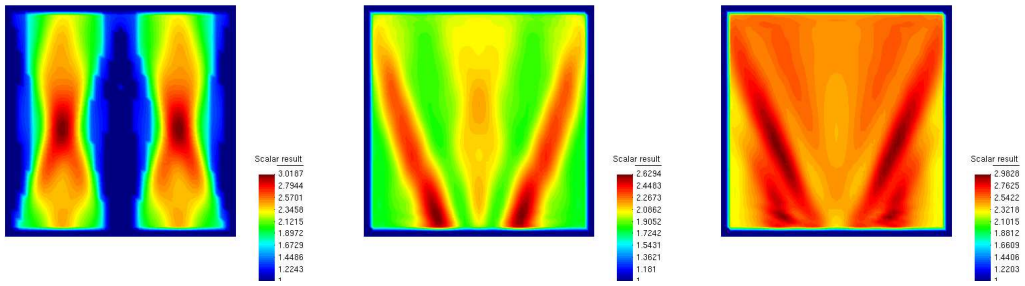

a) b) c)

Figure 15: Test 5: spatial distribution of c_h.

7.4 Conclusions from numerical studies

We have tested our algorithm for three different structures of the medium. In all cases we have not assumed any advanced knowledge of the medium, including the background medium. Our regularization parameters were: the sequences $\{\lambda_n\}_{n=1}^{\overline{N}}$ and $\{\varepsilon_n\}_{n=1}^{\overline{N}}$, as well as iteration numbers n_0 and $\overline{N}$, where n_0 is the iteration number at which relative norms (7.5) of gradients of tails are stabilized and $\overline{N} \in (n_0, N)$ is the total number of functions q_n we have computed. The number $\overline{N}$ is such that the relative norms (7.6) of the unknown coefficient are stabilized. We have used $m_1 = ... = m_{n_0} = 4, m_{n_0+1} = ... = m_{\overline{N}} = 7$ for the number of iterations with respect to tails. Numbers n_0 and $\overline{N}$ were chosen on the basis of an objective stopping rule. So, although they were different for different tests, but the stopping rule remained the same. On the other hand, for $n \in \left[\overline{N}+2, N\right]$ norms (7.5) and (7.6) were abruptly growing. This indicates that our choice of the number of iterations $\overline{N}$ as a regularization parameter was correct one and was in a good agreement with the classic regularization theory, see p. 157 of [11].

It is important that our numerical experiments have *consistently* demonstrated good reconstruction results for the *same* sequences $\{\lambda_n\}_{n=1}^{\overline{N}}$ and $\{\varepsilon_n\}_{n=1}^{\overline{N}}$ of regularization parameters, for the *same objective* stopping rule and for two different noise levels of 5% and 15%. This points towards robustness of our numerical method.

An interesting conclusion can be drawn from the comparison of Figure 6a with Figure 6b, and similarly from the comparison of Figure 12a with Figure 12b. One can observe that the relative errors in final tails are about the same as those in reconstructed coefficients. This provides a numerical confirmation of one of statement of the second remark after Theorem 6.1: that the error of reconstruction is basically $O(\xi)$, where ξ is the truncation error for tails. Results of Test 4 demonstrate this once again. Results of Test 5 demonstrate that a

conventional reconstruction technique might not provide a good image, unless a good first guess for the solution is known.

8 Summary

We have presented a new globally convergent numerical method for a class of multidimensional Coefficient Inverse Problems for some hyperbolic and parabolic PDEs. These inverse problems arise in applications to acoustics, electromagnetics and optical medical imaging. The two key new ideas are: (1) solution of the boundary value problem (3.8), (3.9) for a nonlinear integral differential equation via a layer stripping procedure with respect to the pseudo frequency s, and (2) weakening the influence of the nonlinear term $(\nabla q_n)^2$ via the introduction of $s-$dependent Carleman Weight Functions in the numerical scheme. Unlike this, in all previous works, both theoretical and numerical ones, CWFs were dependent only on spatial variables and were associated with the Carleman estimates for certain differential operators. We have proven a global convergence result, conditions of which are in a good agreement with the classic theory of ill-posed problems.

We have verified our convergence Theorem 6.1 on a number of numerical experiments for an inverse problem of the determination of the coefficient in the principal part of a hyperbolic operator, which means the determination of either the speed of sound, in the case of acoustics, or of the product of the magnetic permeability and electric permittivity coefficients in the case of electromagnetics. In particular, these experiments have demonstrated robustness of our method, which provides good quality images with up to 15% relative random noise in the data. We have also verified numerically the asymptotic behavior (3.4) in all our tests, as well as the positivity of the function w.

We have observed that iterations with respect to tails are very important for the image reconstruction, which was also observed in the previous publication [27] (see section 4 in [27]). In all our numerical experiments the starting value for the tail function was simply zero, which reflects the fact that we do not know a good first guess for the solution. Numerical results demonstrate both robustness of this method and a good quality of reconstructed images, including good quality reconstructions of high contrasts inside of inclusions. The latter is hard to achieve by locally convergent methods. Shapes of inclusions are "smeared" due to three factors. First, the Laplace transform actually leads to a diffusion-like equation for the function w. Second, the ill-posed nature of the original inverse problem quite often causes smeared shapes of reconstructed objects. Third and perhaps the most important one is that we do not know tails. Finally, we have demonstrated numerically that a locally convergent algorithm might result in significantly deteriorated images, unless a good first guess about the solution is given.

Acknowledgments

The work of LB was supported by Project No. IKT 820.94.000 at NTNU, Department of Mathematical Sciences, Trondheim, Norway. The work of MK was supported by the U.S. Army Research Laboratory and U.S. Army Research Office under contract/ grant number W911NF-05-1-0378, as well as by the grant No. 1R21NS052850-01A1 from the National Institutes of Health. The authors are grateful to V.G. Romanov for consulting about smoothness conditions of Theorem 4.1 of [25]. A part of this work was performed during a visit by the authors (November 12-18, 2007) of the Special Semester on Quantative Biology Analyzed by Mathematical Methods, October 1$^{\text{st}}$, 2007 - January 27$^{\text{th}}$, 2008, organized by RICAM, Austrian Academy of Sciences.

References

[1] H. Ammari, E. Iakovleva, and D. Lesselier. Music-type electromagnetic imaging of a collection of small three-dimensional inclusions. *SIAM J.Sci.Comp.*, 29:674–709, 2007.

[2] S. Arridge. Optical tomography in medical imaging. *Inverse Problems*, 15:841–893, 1999.

[3] A. B. Bakushinsky, T. Khan, and A. Smirnova. Inverse problem in optical tomography and its numerical investigation by iteartively regularized methods. *J. Inverse and Ill-Posed Problems*, 13:537–551, 2005.

[4] L. Beilina and C. Clason. An adaptive hybrid fem/fdm method for an inverse scattering problem in scanning acoustic microscopy. *SIAM J. Sci. Comp.*, 28(1):382–402, 2006.

[5] L. Beilina, K. Samuelsson, and K. Åhlander. Efficiency of a hybrid method for the wave equation. In *International Conference on Finite Element Methods*, Gakuto International Series Mathematical Sciences and Applications. Gakkotosho CO.,LTD, 2001.

[6] M. I. Belishev. Boundary control in reconstruction of manifolds and metrics (the bc method). *Inverse Problems*, 13, R1-R45, 1997.

[7] M. I. Belishev and V. Yu Gotlib. Dynamical variant of the bc-method: theory and numerical testing. *J. Inverse and Ill-Posed Problems*, 7:221–240, 1999.

[8] V. A. Burov, S. A. Morozov, and O. D. Rumyantseva. Reconstruction of fine-scale structure of acoustical scatterers on large-scale contrast background. *Acoustical Imaging*, 26:231–238, 2002.

[9] T. Carleman. Sur un proble′me d'unicite′ pur les systee′mes d'e′quations aux de′rivee′s partielles a′ deux varibales inde′ pendantes. *Ark. Mat. Astr. Fys*, 26B(No. 17):1–9, 1939.

[10] Y. Chen. Inverse scattering via heisenberg uncertainty principle. *Inverse Problems*, 13:253–282, 1997.

[11] H. W. Engl, M. Hanke, and A. Neubauer. *Regularization of Inverse Problems*. Kluwer Academic Publishers, Boston, 2000.

[12] B. Engquist and A. Majda. Absorbing boundary conditions for the numerical simulation of waves. *Math. Comp.*, 31:629–651, 1977.

[13] E. Haber, U. M. Asher, and D. Oldenburg. On optimization techniques for solving nonlinear inverse problems. *Inverse Problems*, 16:1263–1280, 2000.

[14] S.I. Kabanikhin, A.D. Satybaev, and M.A. Shishlenin. *Direct Methods of Solving Multidimensional Inverse Hyperbolic Problems.* VSP, The Netherlands, 2004.

[15] M. Klibanov and A. A. Timonov. Numerical studies on the globally convergent convexification algorithm in 2d. *Inverse Problems*, (23):123–138, 2007.

[16] M. V. Klibanov. Inverse problems and carleman estimates. *Inverse Problems*, 8:575–596, 1991.

[17] M. V. Klibanov and A. Timonov. *Carleman Estimates for Coefficient Inverse Problems and Numerical Applications*. VSP, Utrecht, The Netherlands, 2004.

[18] O. A. Ladyzhenskaya, V. A. Solonnikov, and N. N. Uralceva. *Linear and Quasilinear Equations of Parabolic Type*. AMS, Providence, R.I., 1968.

[19] O. A. Ladyzhenskaya and N. N. Uralceva. *Linear and Quasilinear Elliptic Equations*. Academic Press, New York, 1969.

[20] M. M. Lavrentjev, V. G. Romanov, and S. P. Shishatskii. *Ill-posed problems of Mathematical Physics and Analysis*. AMS, 1986.

[21] J. Mueller and S. Siltanen. Direct reconstructions of conductivities from boundary measurements. *SIAM J. Sci. Comp.*, 24:1232–1266, 2003.

[22] A. Nachman. Global uniqueness for a two-dimensional inverse boundary value problem. *Annals of Mathematics*, 143:71–96, 1996.

[23] R. G. Novikov. Multidimensional inverse spectral problem for the equation $-\delta\psi + (v(x) - eu(x))\,\psi = 0$. *Functional Analysis and Its Applications*, 22:11–22, 1988.

[24] R. G. Novikov. The $\overline{\partial}$ approach to approximate inverse scattering at fixed energy in three dimensions. *International Math. Research Papers*, 6:287–349, 2005.

[25] V. G. Romanov. *Inverse Problems of Mathematical Physics*. VNU, Utrecht, The Netherlands, 1986.

[26] J. Schauder. Über lineare elliptische differentialgleichnungen zweiter ordnung. *Math.Z.*, 28:257–282, 1934.

[27] J. Su, H. Shan, H. Liu, and M. V. Klibanov. Reconstruction method from a multiple-site continuous-wave source for three-dimensional optical tomography. *J. Optical Society of America A*, 23:2388–2395, 2006.

[28] A. N. Tikhonov and V. Y. Arsenin. *Solutions of Ill-Posed Problems*. Winston and Sons, Washington, DC, 1977.

[29] J. Xin and M. V. Klibanov. Comparative studies of the globally convergent convexification algorithm with application to imaging of antipersonnel land mines. *Applicable Analysis*, 86:1147–1176, 2007.